LIMITED

Library Circulation Copy
REFERENCE COPY

# Communications Research Centre

# INTERMODULATION ANALYSIS WITH FOURIER-BESSEL EXPANSIONS

by

J.L. Pearce

DEPARTMENT OF COMMUNICATIONS
MINISTÈRE DES COMMUNICATIONS

CRC REPORT NO. 1284

This work was sponsored by the Department of National Defence, Research and Development Branch under Project No. 28-01-31.

IC

CANADA

OTTAWA, MARCH 1976

TK
5102.5
C673e
#1284

COMMUNICATIONS RESEARCH CENTRE

DEPARTMENT OF COMMUNICATIONS
CANADA

# INTERMODULATION ANALYSIS WITH FOURIER-BESSEL EXPANSIONS

by

J.L. Pearce

*(Space Applications Branch)*

Industry Canada
Library - Queen

SEP - 4 2012

Industrie Canada
Bibliothèque - Queen

CRC REPORT NO. 1284
TELS REPORT NO. 31

*Received February 1976*
*Published March 1976*
OTTAWA

**This work was sponsored by the Department of National Defence, Research and Development Branch under Project No. 28-01-31.**

**CAUTION**

**The use of this information is permitted subject to recognition of proprietary and patent rights.**

76-031

TABLE OF CONTENTS

NOTATION . . . . . v

ABSTRACT . . . . . 1

1. INTRODUCTION . . . . . 1

1.1 Background . . . . . 3

2. SINUSOIDAL INTERMODULATION ANALYSIS . . . . . 4

2.1 Intermod Prediction for Sinusoids . . . . . 5

2.2 Angle-Modulated Signals . . . . . 11

3. GAUSSIAN INTERMODULATION ANALYSIS . . . . . 12

3.1 Development . . . . . 12

3.2 Discussion . . . . . 20

4. PREDICTION OF INTERMODULATION NOISE . . . . . 21

4.1 Computer Programs . . . . . 21

4.2 TWT Amplifiers . . . . . 22

5. SOLID STATE AMPLIFIERS . . . . . 26

5.1 Measurement Techniques . . . . . 27

5.2 Dynamic Modeling Technique . . . . . 34

5.3 Multicarrier Intermodulation Performance . . . . . 42

5.4 UHF Solid State Amplifiers - Class C . . . . . 45

5.5 UHF Solid State Amplifiers - Class L . . . . . 51

6. CONCLUDING REMARKS . . . . . 55

7. ACKNOWLEDGEMENTS . . . . . 55

8. REFERENCES . . . . . 55

APPENDIX A - Bessel Function Relationships . . . . . 58

APPENDIX B - Gaussian Sinusoid Development . . . . . 61

APPENDIX C - Equipment List . . . . . 66

## NOTATION

| | |
|---|---|
| $s(\cdot)$ | composite input signal |
| $z(\cdot)$ | composite output signal |
| $\bar{z}$ | complex version of z |
| $\omega_o$ | system centre frequency |
| $x(\cdot)$ | inphase signal component |
| $y(\cdot)$ | quadrature signal component |
| $\bar{g}(\cdot)$ | complex amplifier characteristic |
| $f(\cdot)$ | amplifier phase characteristic |
| $t$ | time |
| $\tau$ | autocorrelation time shift |
| $h(x,y)$ | two dimensional complex nonlinearity |
| $H(\gamma,\xi)$ | two dimensional Fourier transform of h(x,y) |
| $A_\ell$ | $\ell^{th}$ user signal amplitude |
| $\theta_\ell(\cdot)$ | $\ell^{th}$ user signal phase |
| $N$ | total number of users |
| $J_\nu$ | $\nu^{th}$ order Bessel function |
| $I_\nu$ | $\nu^{th}$ order modified Bessel function |
| $\bar{a}_k$ | $k^{th}$ complex Fourier-Bessel series expansion coefficient |
| $\Omega_k$ | $k^{th}$ positive zero of $J_\nu(\cdot)$ |
| $\rho$ | composite input signal amplitude |
| $R_z(\cdot)$ | autocorrelation function of z |
| $\mu_\ell(\cdot)$ | $\ell^{th}$ user angle modulation |
| $\phi(\cdot)$ | input signal autocorrelation function amplitude |
| $\Lambda(\cdot)$ | input signal autocorrelation function phase |
| $\omega_\ell$ | $\ell^{th}$ user channel frequency shift |

# INTERMODULATION ANALYSIS WITH FOURIER-BESSEL EXPANSIONS

by

J.L. Pearce

ABSTRACT

In any frequency-division-multiple-access (FDMA) satellite communications system the control of intermodulation noise must be considered if all signals are amplified by a single nonlinear power amplifier in the satellite transponder.

The subject of this report is the use of Fourier-Bessel series expansion models in the prediction of the intermodulation performance of both travelling-wave-tube (TWT) amplifiers and solid state class C, UHF amplifiers. Both theoretical and experimental results are described and compared.

It is shown that in the case of the solid state amplifiers a dynamic characteristic measurement technique must be used before reliable predictions can be achieved. A simple intermodulation noise reduction scheme is described for use with high-power-efficiency-class-C solid state amplifiers. It is demonstrated that a signal-to-intermodulation noise power ratio improvement of 10 dB can be achieved with a minimal decrease in prime power efficiency.

## 1. INTRODUCTION

Prime electrical power is an expensive commodity onboard a satellite. For this reason the final power amplifier of the communication transponder is usually operated in a power-efficient but nonlinear mode. If the satel-

lite is part of an FDMA (frequency-division multiple-access) communication system, intermodulation noise can be of sufficient strength so as to degrade normal channel operation. To avoid channel degradation it is necessary either to use a linear satellite transponder or to control the operation of a nonlinear transponder so as to reduce the effect of the intermodulation noise to an acceptable level.

A preliminary indication of the significance of the intermodulation noise can be obtained if it is assumed its effect is to augment the background system noise level. A system with a nonlinear amplifier, and hence intermodulation noise, will require a greater satellite output signal power level than if a linear amplifier is used if the same final signal-to-noise power ratio is to be maintained at the ground receive station. This does not necessarily mean that more satellite prime power is required since, for example, a nonlinear class-C amplifier is generally considerably more efficient than a class-A linear amplifier. The change in prime power requirements is plotted in Figure 1 as a function of the ratio of signal-to-intermodulation ratio and required signal-to-noise ratio, with amplifier efficiency ratio as a parameter. From the curve for $\rho = 1$ (both amplifiers have the same prime power-efficiency), it is evident that if the signal-to-intermodulation ratio exceeds the required signal-to-noise ratio by 10 dB, the excess prime power requirement is less than 0.5 dB. When it is realized that the power efficiency of a nonlinear amplifier is usually greater (e.g., $\rho = 0.4$) than that of a linear amplifier, it is evident that a potential saving in amplifier prime power requirement exists. The reduction achievable depends upon the relative power levels of the system noise and intermodulation noise. In order to select a set of acceptable operating parameters for a nonlinear amplifier it is necessary to be able to predict intermodulation noise levels for specific amplifiers.

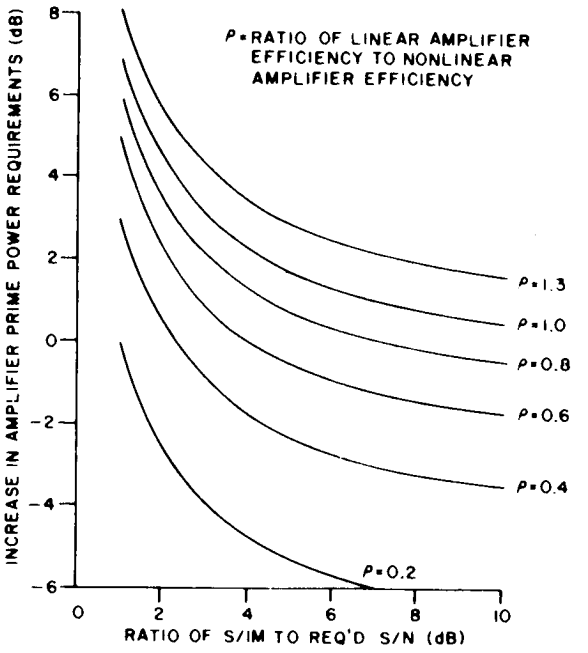


*Figure 1. Satellite Prime Power Requirements*

In this report it is assumed the nonlinear amplifiers under consideration are memoryless, exhibit a nonlinear amplitude transfer characteristic and convert any amplitude modulation into a phase modulation (AM-PM conversion) in a nonlinear fashion. These amplifiers are modeled by a complex Fourier-Bessel series expansion. Mathematical relationships are then developed to permit the prediction of the required intermodulation noise levels. A dynamic experimental measurement technique is described to measure the characteristics of solid state UHF amplifiers.

Finally, predicted and measured intermodulation levels are discussed and compared for various amplifiers. This technique is dynamic in the sense that the power of the inserted test signal is automatically swept over the range of values of interest.

The work presented in this report permits the prediction of intermodulation levels when many modulated signals are amplified by a single nonlinear amplifier. Specific results are presented for combinations of digital PSK and FSK signals, sinusoids and combinations of signals with a constant power spectrum over a specified frequency range.

## 1.1 BACKGROUND

Most of the intermodulation analysis to date is based upon the nonlinear transform analysis technique originated by Rice [1] and subsequently described by Davenport and Root [2]. The notable exceptions to this technique are the use of a power series to model the nonlinear characteristic as used by Eric [3], a Fourier series model as used by Berman and Podraczky [4] and an error-function model, described by Baum [5] and used by Pawula et al. [6] and Pawula [7]. The analysis in this report makes use of the transform analysis technique.

A number of the published papers consider the input signal to be a sum of sinusoids plus additive gaussian noise. In particular, Davenport [8] considers a single sinusoid plus noise, Jones [9] considers two sinusoids plus noise and Shaft [10] considers an unspecified number of sinusoids plus noise. All of these authors make use of the transform analysis technique and model the nonlinear amplifier by an amplitude hard limiter. Two serious shortcomings of the above papers are that they do not consider the phase conversion of any amplitude modulation (AM-PM conversion) on the input signal and they are insensitive to particular device characteristics. Notwithstanding these shortcomings, these papers contain an excellent documentation of the nonlinear amplification effects for one to four sinusoids.

Shimbo [11] in his analysis considers the effects of AM-PM conversion and suggests the use of various series expansions to represent the nonlinear amplifier characteristics. Although his results are directly applicable to the analysis of sinusoidal inputs it is not obvious how a general input signal should be handled. Shimbo does present experimental results for the two carrier input situation which agree very well with his predicted intermodulation distortion levels.

A conceptually good model of a general bandpass nonlinearity is presented by Kaye, George and Eric [12] in their quadrature model. Their

analysis considers both an amplitude nonlinearity and AM-PM conversion. They suggest the use of a Fourier-Bessel series expansion to represent the in-phase and quadrature envelope nonlinear characteristics. As they illustrate, use of this type of an expansion leads to a very simple relationship between the envelope characteristic of the device and its instantaneous voltage nonlinear characteristic. A similar type of series expansion will be used in this report since it greatly simplifies the analysis. The analysis used by Kaye et al. [12] is generally applicable where the total input signal is approximately gaussian in nature and has a power spectral density which is symmetrical about the carrier frequency. The gaussian analysis presented in this report supplies a different point of view from Kaye's analysis as well as removes the constraint of symmetry about the carrier frequency. Kaye et al. [12] supply an estimate of the signal-to-interference ratio at the centre of the bandpass when the input power spectral density is constant across the bandpass. Their analysis is extendable to other spectral shapes but it is felt that the more general result presented in this report is no more difficult to implement on a digital computer.

The work of Shimbo [11] has been extended to make use of the Fourier-Bessel series expansion model first suggested by Kaye et al. [12]. This extension is reported in a report by Fuenjalida, Shimbo and Cook [13]. The sinusoidal intermodulation analysis presented in Section 2 of this report is similar to that of Fuenjalida et al. [3]. Unfortunately this analysis approach suffers from a rapidly increasing computing time requirement as the number of input signals increases. To avoid this problem the analysis approach of Section 3 was devised. In this work the composite input signal is assumed to be normally distributed while having a general power spectral shape. The Fast-Fourier Transform algorithm (FFT) is utilized to produce computation times which are essentially independent of the number of individual input signals (if the frequency resolution is allowed to vary). This analysis technique, unlike the FFT analysis of Loo [14], permits the direct prediction of intermodulation and signal terms and is not a simulation type of technique.

The development of section 2 is presented for the sake of completeness of the report. The reader who is familiar with the work of Fuenjalida et al. [13] should proceed to section 3. The reader who wishes to avoid the mathematical details should proceed to section 4.

## 2. SINUSOIDAL INTERMODULATION ANALYSIS

One conventional technique of system analysis is to examine the performance of a system when it is required to transmit a sum of independent sinusoids. In this section, equations are developed for the prediction of signal and intermodulation noise power levels at the output a nonlinear amplifier.

The analysis of this section is of limited value when large numbers of signals (greater than 10) are under consideration since computing time becomes excessive. For this situation the analysis of Section 3 should be used.

## 2.1 INTERMOD PREDICTION FOR SINUSOIDS

In general, the composite, narrowband, bandpass signal at the input to a satellite's nonlinear power amplifier will consist of the sum of the signals from individual users as well as additive noise. The results presented in this report will be for the noiseless case. This composite signal may be represented by

$$s(t) = r(t) \cos \{\omega_o t + \theta(t)\} \tag{2.1}$$

or

$$s(t) = x(t) \cos \omega_o t - y(t) \sin \omega_o t \tag{2.2}$$

Most wideband satellite transponder amplifiers, such as solid state UHF amplifiers, will cause the envelope of the input signal to be modified in a nonlinear fashion as well as convert any amplitude modulation into a phase modulation (AM-PM conversion). This nonlinear transfer characteristic can be represented mathematically by expressing the amplifier's output signal as

$$z(t) = g\{r(t)\} \cos \{\omega_o t + \theta(t) + f[r(t)]\} \tag{2.3}$$

or

$$z(t) = g\{r(t)\} \cos \{f[r(t)]\} \cos\{\omega_o t + \theta(t)\} - g\{r(t)\} \sin\{f[r(t)]\} \sin\{\omega_o t + \theta(t)\} \tag{2.4}$$

where

$g\{r\}$ = the amplifier's nonlinear amplitude conversion characteristic

$f\{r\}$ = the amplifier's nonlinear AM-PM conversion characteristic

Equation (2.4) is a mathematical description of the quadrature model suggested by Kaye et al. [12].

In contrast to the approach used by Kaye et al. [12] a complex signal notation is now introduced. This notation will expedite the analysis to follow. Thus,

$$\bar{s}(t) = [x(t) + jy(t)] \exp j\omega_o t \tag{2.5}$$

or

$$\bar{s}(t) = r(t) \exp j [\omega_o t + \theta(t)] \tag{2.6}$$

and

$$\bar{g}(r) = g(r) \exp j [f(r)] \tag{2.7}$$

where

$$s(t) = \mathrm{Re}\{\bar{s}(t)\} \tag{2.8}$$

$$\mathrm{Re}\{a\} = \text{real part of "a"} \tag{2.9}$$

The amplifier's nonlinear transfer characteristic is represented in complex notation by equation (2.7).

The reader may easily verify that

$$z(t) = \mathrm{Re}\{\bar{z}(t)\} \tag{2.10}$$

given that

$$\bar{z}(t) = \frac{\bar{g}(r)}{r}\,\bar{s}(t) \tag{2.11}$$

or if equations (2.5) and (2.11) are combined

$$\bar{z}(t) = \bar{g}(|x+jy|) \times \frac{(x+jy)}{|x+jy|}\,\exp j\omega_o t \tag{2.12}$$

Equation (2.12) is an expression for the complex version of the nonlinear amplifier's output signal.

At this point it is convenient to introduce the transform nonlinear analysis technique of Rice [1] and Davenport and Root [2] by defining the two-dimensional complex nonlinearity

$$h(x,y) = \bar{g}\{|x+jy|\} \times \frac{(x+jy)}{|x+jy|} \tag{2.13}$$

It now follows directly that

$$h(x,y) = \frac{1}{(2\pi)^2} \iint_{-\infty}^{\infty} H(\gamma,\xi)\,\exp\{j\gamma\, x(t) + j\xi y(t)\}\,d\gamma d\xi \tag{2.14}$$

where

$$H(\gamma,\xi) = \iint_{-\infty}^{\infty} \bar{g}\{|a+jb|\}\,\frac{(a+jb)}{|a+jb|}\,\exp -\{j\gamma a + j\xi b\}\,dadb \tag{2.15}$$

Here it is assumed all integrals exist and are convergent. If not, it is assumed that the nonlinearity, $\bar{g}(r)$ can be modified by the use of a window function so that existance and convergence are not a problem. The function $H(\gamma,\xi)$, as defined in equation (2.15) is a two-dimensional Fourier transform of the complex nonlinearity $\bar{g}(r)$ while equation (2.14) is the corresponding inverse transform. An expression for the amplifier output signal follows directly from equations (2.12), (2.13) and (2.14) as

$$\bar{z}(t) = \frac{1}{4\pi^2} \exp j\omega_o t \iint_{-\infty}^{\infty} H(\gamma,\xi) \exp\{j\gamma x(t) + j\xi y(t)\} \, d\gamma d\xi \tag{2.16}$$

Examine now the signal components $x(t)$ and $y(t)$, defined implicitly by equations (2.5) and (2.6). If it is assumed the individual user component signals can be represented by

$$\{A_\ell \cos(\omega_o t + \theta_\ell) \quad : \quad \ell = 1,2,3,\ldots,N\} \tag{2.17}$$

N = total number of input signals

then it follows directly that

$$x(t) = \sum_{\ell=1}^{N} A_\ell \cos \theta_\ell \tag{2.18}$$

$$y(t) = \sum_{\ell=1}^{N} A_\ell \sin \theta_\ell \tag{2.19}$$

For sinusoidal user signals

$$\theta_\ell = \omega_\ell t \tag{2.20}$$

where the user carrier frequency is given by $(\omega_o + \omega_\ell)$. For angle-modulated signals

$$\theta_\ell = \omega_\ell t + m_\ell(t) \tag{2.21}$$

A combination of equations (2.18) and (2.19) with equation (2.16) yields the following expression

$$\bar{z}(t) = \frac{1}{4\pi^2} \exp j\omega_o t \iint_{-\infty}^{\infty} H(\gamma,\xi) \prod_{\ell=1}^{N} \exp\{j\gamma A_\ell \cos\theta_\ell + j\xi A_\ell \sin\theta_\ell\} \, d\gamma d\xi \tag{2.22}$$

where the symbol $\Pi$ is used to indicate a multiple product. Trigonometry can now be used to express the exponential term in the form

$$\exp\left\{ jA_\ell |\gamma + j\xi| \sin\left[\theta_\ell + \arctan\left(\frac{\gamma}{\xi}\right)\right]\right\} \tag{2.23}$$

This expression (2.23) can be expanded using Jacobi's expansion (see A.17, Appendix A) so that the complex output signal can be expressed as

$$\bar{z}(t) = \frac{1}{4\pi^2} \exp j\omega_o t \iint_{-\infty}^{\infty} H(\gamma,\xi) \prod_{\ell=1}^{N} \sum_{n=-\infty}^{\infty} J_n(A_\ell|\gamma+j\xi|)\exp\left\{jn\left[\theta_\ell + \arctan\left(\frac{\gamma}{\xi}\right)\right]\right\} d\gamma d\xi \tag{2.24}$$

The expression in equation (2.24) consists of a product of summations, the order of which can be reversed if the single summation is replaced by N nested summations of product terms. If at the same time equation (2.15) is substituted for $H(\gamma,\xi)$ the output signal expression reduces to

$$\bar{z}(t) = \frac{1}{4\pi^2} \exp j\omega_o t \iiiint_{-\infty}^{\infty} \sum_{n_\ell=-\infty}^{\infty} \left\{\prod_{\ell=1}^{N} J_{n_\ell}(A_\ell|\gamma+j\xi|)\right\} \exp\left\{j \sum_{\ell=1}^{N} n_\ell\left[\theta_\ell + \arctan\left(\frac{\gamma}{\xi}\right)\right]\right\}$$

$$\times \bar{g}(|a+jb|) \frac{(a+jb)}{|a+jb|} \exp\{-j\gamma a - j\xi b\}\, d\gamma d\xi\, da db \tag{2.25}$$

The symbol $\sum_{n_\ell=-\infty}^{\infty}$ is used to represent the nested summations, one for each value of "$\ell$".

At this point in the analysis it is useful to convert to a polar co-ordinate systems through the following transformations

$$\begin{aligned} a &= \rho \cos\eta & \xi &= \alpha \cos\beta \\ b &= \rho \sin\eta & \xi &= \alpha \sin\beta \end{aligned} \tag{2.26}$$

thus

$$\begin{aligned} \gamma a + \xi b &= \rho\alpha\{\cos\eta \sin\beta + \sin\eta \cos\beta\} \\ &= \rho\alpha \sin\{\eta + \beta\} \end{aligned} \tag{2.27}$$

and hence

$$\bar{z}(t) = \frac{1}{4\pi^2} \exp j\omega_o t \sum_{n_\ell=-\infty}^{\infty} \exp\left\{j \sum_{\ell=1}^{N} n_\ell\theta_\ell\right\} \int_0^{\infty}\int_{-\pi}^{\pi} \left\{\prod_{\ell=1}^{N} \alpha J_n(A_\ell\alpha)\right\} \exp\left\{j \sum_{\ell=1}^{N} n_\ell\beta\right\}$$

$$\times \rho\bar{g}(\rho) \exp j\{\eta - \rho\alpha \sin(\eta+\beta)\}\, d\eta d\beta d\alpha d\rho \tag{2.28}$$

Although it may appear on the surface this expression is more complex than previous versions, this is not the case. It is now possible by the use of Bessel's integral (see equation A.1, Appendix A) to perform the integration with respect to the angular variable $\eta$ to get

$$\bar{z}(t) = \frac{1}{2\pi} \exp j\omega_o t \sum_{n_\ell=-\infty}^{\infty} \exp\left\{ j \sum_{\ell=1}^{N} n_\ell \theta_\ell \right\} \iiint_{o-\pi}^{\infty \quad \pi} \left\{ \prod_{\ell=1}^{N} \alpha J_{n_\ell} (A_\ell \alpha) J_1(\alpha\rho)\rho\, \bar{g}(\rho) \right\}$$

$$\times \exp\left\{ j \left( \sum_{\ell=1}^{N} n_\ell - 1 \right) \beta \right\} d\beta d\rho d\alpha \qquad (2.29)$$

Examine now the integration with respect to $\beta$. The above expression gives a zero value for $\bar{z}(t)$ in all cases except when

$$\sum_{\ell=1}^{N} n_\ell = 1 \qquad (2.30)$$

in which case the expression in equation (2.29) reduces to

$$\bar{z}(t) = \exp j\omega_o t \sum_{n_\ell=-\infty}^{\infty} \exp\left\{ j \sum_{\ell=1}^{N} n_\ell \theta_\ell \right\} \iint_{o}^{\infty} \prod_{\ell=1}^{N} \alpha J_{n_\ell} (A_\ell \alpha) J_1(A_\ell \alpha) \rho \bar{g}(\rho)\, d\alpha d\rho \qquad (2.31)$$

This expression can be reduced to a simple form if the nonlinear amplifier is modeled by a Fourier-Bessel series expansion, that is,

$$\bar{g}(\rho) = \sum_{k=1}^{\infty} \bar{a}_k J_\nu(\Omega_k \rho) \qquad (2.32)$$

where

$\bar{a}_k$ = complex coefficients

$\Omega_k$ = the positive zeros of $J_\nu(x)$ arranged in order of ascending magnitude

The coefficients $\bar{a}_k$ can be expressed as an integral of a product function of $\bar{g}(\xi)$ and $J_\nu(\Omega_k \xi)$ [15] although this approach will not be used. It is interesting to observe that expansions similar to equation (2.32) have proved useful in studies of heat conduction and mechanical vibration [15].

The expression for the output signal, $\bar{z}(t)$ becomes

$$\bar{z}(t) = \exp j\omega_o t \sum_{n_\ell=-\infty}^{\infty} \exp\left\{ j \sum_{\ell=1}^{N} n_\ell \theta_\ell \right\} \int_o^\infty \alpha \left\{ \prod_{\ell=1}^{N} J_{n_\ell}(A_\ell \alpha) \right\} \int_o^\infty \rho J_1(\alpha\rho) \sum_{k=1}^{\infty} \bar{a}_k J_\nu(\Omega_k \rho) d\rho d\alpha \tag{2.33}$$

If the constraint $\nu = 1$ is applied to the series expansion of equation (2.32), the integrals in equation (2.33) can be put into the form of Hankel's repeated integral which can be evaluated by equation (A.7) in Appendix A. Equation (2.33) reduces to

$$\bar{z}(t) = \exp(j\omega_o t) \sum_{n_\ell=-\infty}^{\infty} \exp\left\{ j \sum_{\ell=1}^{N} n_\ell \theta_\ell \right\} \left\{ \sum_{k=1}^{\infty} \bar{a}_k \prod_{\ell=1}^{N} J_{n_\ell}(\Omega_k A_\ell) \right\} \tag{2.34}$$

The reader must recall at this stage that the summation with respect to $n_\ell$ is a nested summation.

It is instructive to pause a moment to study equation (2.34). The reader will observe that

1. the "nonlinear terms" are separated from the signal modulation terms,
2. the expression of equation (2.34) is valid for all angle-modulated signal types where

$$\theta_\ell(t) = \omega_\ell t + \mu_\ell(t) \tag{2.35}$$

where

$\omega_\ell$ = user frequency shift from the reference frequency of $\omega_o$

$\mu_\ell(t)$ = the user's angle modulation

For sinusoids it is assumed there is no modulation and hence $\mu_\ell(t) = \mu_\ell$ = initial phase of the carrier.

The frequency of any particular component is given by

$$\omega(n_\ell: \ \ell = 1,2,\ldots,N) = \omega_o + \sum_{\ell=1}^{N} n_\ell \omega_\ell \tag{2.36}$$

while the power contained in this component is given by

$$M(n_\ell: \ \ell = 1,2,\ldots,N) = \frac{1}{2} \left| \sum_{k=1}^{\infty} \bar{a}_k \prod_{\ell=1}^{N} J_{n_\ell}(\Omega_k A_\ell) \right|^2 \tag{2.37}$$

The i'th signal component is obtained for $n_i = 1$ and $n_\ell = 0 : \ell \neq i$. From equations (2.36) and (2.37) it is possible to determine the signal and intermodulation power levels on any frequency of interest for the specific amplifier represented by the coefficient set $\{\bar{a}_k : k = 1, 2....\}$.

A computer implementation of this analysis technique will be discussed in a later section.

## 2.2 ANGLE-MODULATED SIGNALS

Consider for a moment the situation when the carriers are modulated. The autocorrelation function of the complex output signal is

$$\bar{R}(\tau) = E\{\bar{z}^*(t)\bar{z}(t+\tau)\} \tag{2.38}$$

where: E[x] denotes an ensemble average of x

The autocorrelation of Z(t), or the real output signal is

$$R_z(\tau) = \frac{1}{2} \mathrm{Re}\{\bar{R}(\tau)\} \tag{2.39}$$

These last two equations assume the process $\bar{z}(t)$ is at least wide-sense stationary. If the user modulation, given by equation (2.35) is substituted into equation (2.34) it is possible to express the autocorrelation function of equation (2.38) as

$$\bar{R}(\tau) = \sum_{n_\ell=-\infty}^{\infty} \left\{ \sum_{k=1}^{\infty} \bar{a}_k \prod_{\ell=1}^{N} J_{n_\ell}(\Omega_k A_\ell) \right\} \exp j \left\{ \left( \omega_o + \sum_{\ell=1}^{N} n_\ell \omega_\ell \right) \tau \right\} \times \prod_{\ell=1}^{N} E[\exp j n_\ell \{\mu_\ell(t+\tau) - \mu_\ell(t)\}] \tag{2.40}$$

This expression is essentially the same as that presented by Shimbo [11] and Fuenzalida [13]. Although this is a relatively simple expression there are two significant difficulties with its use. Firstly, the number of permissible sets of $\{n_\ell : \ell = 1, 2....N\}$ values becomes excessively large very quickly as the number of carriers N increases (and hence the computation time increase rapidly). Secondly, the ensemble average indicated in equation (2.40) is often not readily available although a similar average has been investigated for binary FSK signals by Wittke [16] in his studies of power spectra.

In order to avoid these difficulties the analysis of Section 3 might be used. This analysis assumes that the individual carriers are approximately power balanced and that they are present in sufficient numbers that the composite signal may be modeled by a gaussian process. No assumption is made concerning the individual user power spectral shapes.

# 3. GAUSSIAN INTERMODULATION ANALYSIS

As noted previously the analysis of Section 2 results in a rapidly increasing computation time as the number of carriers increases. A practical limit on the number of carriers appears to be of the order of ten.

In most satellite communication systems using FDMA an attempt is usually made to keep the uplink signal powers approximately equal among the various users. If the number of uplink signals is in excess of ten it is reasonable to assume the central limit theorem can be applied and the composite satellite input signal modeled by a gaussian stochastic process. The analysis which follows makes this assumption and results in computer programs for which the execution times are essentially independent of the number of carriers. An additional advantage is that the input signal power spectral shape is allowed to be completely general.

## 3.1 DEVELOPMENT

The notation of Section 2 will be continued in this section. Thus, with reference to equation (2.38), the complex output autocorrelation function is

$$\bar{R}(\tau) = E\{\bar{z}^*(t)\bar{z}(t+\tau)\} \tag{3.1}$$

where the autocorrelation function of the amplifier output signal is

$$R_z(\tau) = \frac{1}{2}\,\mathrm{Re}\{\bar{R}(\tau)\} \tag{3.2}$$

For notational simplicity define

$$\bar{z}_1(t) = \bar{z}(t)$$

$$\bar{z}_2(t) = \bar{z}(t+\tau) \tag{3.3}$$

If equations (2.12) and (3.1) are combined it is evident that

$$\bar{R}(\tau) = \exp j\omega_o\tau\, E\left[\bar{g}\{|x_2 + jy_2|\}\,\frac{(x_2+jy_2)}{|x_2+jy_2|} \times \bar{g}^*\{|x_1-jy_1|\}\,\frac{(x_1-jy_1)}{|x_1-jy_1|}\right] \tag{3.4}$$

This expression is a cross-correlation of the signals at the output of the two nonlinearities $\bar{g}(s_2)$ and $\bar{g}^*(s_1)$, as observed by Pawula [7].

Once again the nonlinear analysis technique of Rice [1] and Davenport and Root [2] can be applied as in Section 2. With reference to the defining equations (2.13) and (2.15) for $H(\gamma,\xi)$ let

$$H_1(\gamma_2,\xi_2) = H(\gamma_2,\xi_2) \tag{3.5}$$

This redefinition of $H(\gamma,\xi)$ is used for clarity in the following development.

In a similar fashion the two-dimensional Fourier Transform of the complex conjugate of equation (2.13) can be defined as $H_2(\gamma,\xi)$. A combination of equations (3.4), (2.13) and (2.14) results in the following expression for the complex autocorrelation function:

$$\bar{R}(\tau) = \frac{1}{(2\pi)^4} \exp j\omega_o\tau \int\int\int\int_{-\infty}^{\infty} H_1(\gamma_2,\xi_2)H_2(\gamma_1,\xi_1)$$

$$\times E\left[\exp\{j\gamma_1 x_1 + j\xi_1 y_1 + j\gamma_2 x_2 + j\xi_2 y_2\}\right] d\gamma_1 d\gamma_2 d\xi_1 d\xi_2 \tag{3.6}$$

Let the joint characteristic function of $x_1$, $y_1$, $x_2$, $y_2$ be $M(\gamma_1, \xi_1, \gamma_2, \xi_2)$. Equation (3.6) can now be written as

$$\bar{R}(\tau) = \frac{1}{(2\pi)^4} \exp j\omega_o\tau \int\int\int\int_{-\infty}^{\infty} H_1(\gamma_2,\xi_2)H_2(\gamma_1,\xi_1)M(\gamma_1,\xi_1,\gamma_2,\xi_2)\, d\gamma_1, d\gamma_2 d\xi_1 d\xi_2 \tag{3.7}$$

Evaluation of equation (3.7) is the subject of this section.

Consider for the moment the transform expression of equation (2.15) and in particular convert the rectilinear co-ordinates (a, b) and $(\gamma,\xi)$ into the polar co-ordinates $(\rho,\eta)$ and $(\alpha,\beta)$ respectively by the transformations

$$\begin{aligned} a &= \rho \cos \eta \qquad & b &= \rho \sin \eta \\ \gamma &= \alpha \cos \beta \qquad & \xi &= \alpha \sin \beta \end{aligned} \tag{3.8}$$

Let $H_{1\rho}(\alpha,\beta)$ be $H_1(\gamma,\xi)$ with the independent variables expressed as polar co-ordinates. It now follows directly from equation (2.15) that

$$H_{1\rho}(\alpha_1,\beta_1) = \int_0^{\infty}\int_{-\pi}^{\pi} \rho_1 \bar{g}(\rho_1) \exp j\{\eta_1 - \alpha_1\rho_1 \cos(\eta_1-\beta_1)\}\, d\eta_1 d\rho_1 \tag{3.9}$$

The integration with respect to $\eta$ can be performed by an application of the general form of Bessel's integral given by equation (A.4) in Appendix A. The result is that

$$H_{1\rho}(\alpha_2,\beta_2) = -2\pi j \exp\{j\beta_2\} \int_0^{\beta} \rho \bar{g}(\rho_1) J_1(\alpha_2\rho_2) d\rho_2 \tag{3.10}$$

By a similar development, making use of equation (A.5) instead of equation (A.4), it can be shown that

$$H_{2\rho}(\alpha_1,\beta_1) = -2\rho j \exp\{-j\beta_1\} \int_0^\infty \rho_1 \overline{g}^{*}(\rho_1) J_1(\alpha_1\rho_1) d\rho_1 \tag{3.11}$$

Return now to the general expression of equation (3.7). This expression can be converted into a polar co-ordinate form by the basic transformations of equation (3.8) and allowing the joint characteristic function, in polar form, to be represented by $M_\rho(\alpha_1, \beta_1, \alpha_2, \beta_2)$. If this conversion is performed and the simplifications of equations (3.10) and (3.11) introduced the complex autocorrelation function reduces to

$$\overline{R}(\tau) = -\frac{1}{(2\pi)^2} \exp j\omega_o\tau \int_0^\infty\int_{-\pi}^{\pi} \exp\{j(\beta_2-\beta_1)\}\ \alpha_1\alpha_2\ M_\rho(\alpha_1,\beta_1,\alpha_2,\beta_2) d\beta_1 d\beta_2$$

$$\times \int_0^\infty \rho_1 J_1(\alpha_1\rho_1)\overline{g}^{*}(\rho_1) d\rho_1 \int_0^\infty \rho_2 J_1(\alpha_2\rho_2)\overline{g}(\rho_2) d\rho_2 d\alpha_1 d\alpha_2 \tag{3.12}$$

At this point in the development it is necessary to digress and consider the joint characteristic function in more detail. Since the composite input signal is the result of a summation of many individual user signals, it is reasonable to make the assumption that the composite signal tends to exhibit gaussian statistical characteristics. With this assumption it is possible to write the characteristic function, as given by Davenport and Root [2], in the form

$$M(\gamma_1,\xi_1,\gamma_2,\xi_2) = \exp\left[-\frac{1}{2}\left\{\gamma_1^2 E[x_1^2] + \gamma_2^2\ E[x_2^2] + \xi_1^2\ E[y_1^2] + \xi_2^2\ E[y_2^2]\right.\right.$$
$$+ 2\gamma_1\gamma_2\ E[x_1x_2] + 2\xi_1\xi_2\ E[y_1y_2]$$
$$\left.\left. + 2\gamma_1\xi_2\ E[x_1y_2] + 2\gamma_2\xi_1\ E[y_1x_2]\right\}\right] \tag{3.13}$$

To obtain an expression for the expected values within the exponential it is necessary to examine in detail a general bandpass process as described by equations (2.2) and (2.5). The signal represented in equation (2.5) is an analytic signal possessing only positive frequencies provided the bandwidth of the modulation is less than the carrier frequency. This condition exists in all practical satellite transponders. Since $\overline{s}(t)$ is a single-sideband signal it is possible to use an analytic signal representation as given by Schwartz, Bennett and Stein [17] as

$$\overline{s}(t) = s(t) + j\hat{s}(t) \tag{3.14}$$

where $s(t)$ is the signal defined by Equation (2.1) and $\hat{s}(t)$ is the Hilbert Transform of this signal.

It now follows directly from equations (2.5) and (3.14) that

$$x(t) + jy(t) = [s(t) + j\hat{s}(t)] \exp\{-j\omega_o t\} \tag{3.15}$$

which reduce to the two equations

$$x(t) = s(t) \cos \omega_o t + \hat{s}(t) \sin \omega_o t \tag{3.16}$$

$$y(t) = \hat{s}(t) \cos \omega_o t - s(t) \sin \omega_o t \tag{3.17}$$

From these two equations and making use of the Hilbert Transform relationship given by Franks [18] it is evident that

$$E[x_1 x_2] = R(\tau) \cos \omega_o \tau + \hat{R}(\tau) \sin \omega_o \tau \tag{3.18}$$

$$E[y_1 y_2] = E[x_1 x_2] \tag{3.19}$$

$$E[x_1 y_2] = \hat{R}(\tau) \cos \omega_o \tau - R(\tau) \sin \omega_o \tau \tag{3.20}$$

$$E[x_2 y_1] = - E[x_1 y_2] \tag{3.21}$$

when we define $R(\tau)$ by the equation

$$R(\tau) = E[s(t)s(t + \tau)] \tag{3.22}$$

and $\hat{R}(\tau)$ as the Hilbert Transform of $R(\tau)$.

The expectations of Equations (3.18) through (3.21) can now be substituted into the joint characteristic function of equation (3.13) to give

$$\begin{aligned} M(\gamma_1,\xi_1,\gamma_2,\xi_2) = \exp \Bigg[ - \frac{1}{2} \Big\{ & R(o)[\gamma_1^2 + \gamma_2^2 + \xi_1^2 + \xi_2^2] \\ & + 2[R(\tau)\cos \omega_o \tau + \hat{R}(\tau) \sin \omega_o \tau][\gamma_1\gamma_2 + \xi_1\xi_2] \\ & + 2[\hat{R}(\tau) \cos \omega_o \tau - R(\tau) \sin \omega_o \tau][\gamma_1\xi_2 - \gamma_2\xi_1] \Big\} \Bigg] \end{aligned} \tag{3.23}$$

An application of the rectilinear to polar co-ordinate conversion, expressions (3.8), reduces this joint characteristic function to

$$\begin{aligned} Mp(\alpha_1,\beta_1,\alpha_2,\beta_2) = \exp \Bigg[ - \frac{1}{2} \Big\{ & R(o)[\alpha_1^2 + \alpha_2^2] \\ & + 2\alpha_1\alpha_2[R(\tau)\cos \omega_o \tau + \hat{R}(\tau)\sin \omega_o \tau]\cos(\beta_1-\beta_2) \\ & + 2\alpha_1\alpha_2[\hat{R}(\tau)\cos \omega_o \tau - R(\tau)\sin \omega_o \tau]\sin(\beta_2-\beta_1) \Big\} \Bigg] \end{aligned} \tag{3.24}$$

Since the input signal s(t) is a bandpass signal it is evident that the autocorrelation of this signal can be represented in the form

$$R(\tau) = \phi_x(\tau)\cos \omega_o\tau + \phi_y(\tau)\sin \omega_o\tau \tag{3.25}$$

It should be noticed at this point that this general representation must be used since $R(\tau)$ is the autocorrelation of the composite signal and as a result the power spectral density corresponding to $R(\tau)$ may not be symmetrical about the centre frequency $\omega_o$. From equation (3.25) it follows that

$$\hat{R}(\tau) = \phi_x(\tau)\sin \omega_o\tau - \phi_y(\tau)\cos \omega_o\tau \tag{3.26}$$

where it has been assumed $\phi_x(\tau)$ and $\phi_y(\tau)$ are narrowband quantities as compared to $\omega_o$.

Introduction of equations (3.25) and (3.26) into equation (3.24) results in the following expression for the joint characteristic function.

$$Mp(\alpha_1,\beta_1,\alpha_2,\beta_2) = \exp\left[-\frac{1}{2}\left\{\phi_x(o)[\alpha_1^2 + \alpha_2^2] + 2\alpha_1\alpha_2[\phi_x(\tau)\cos(\beta_1-\beta_2) + \phi_y(\tau)\sin(\beta_1-\beta_2)]\right\}\right] \tag{3.27}$$

The composite input autocorrelation function of equation (3.25) can now be expressed in the form

$$R(\tau) = \phi(\tau)\cos\left\{\omega_o\tau + \Lambda(\tau)\right\}$$

$$= \phi_x(\tau)\cos \omega_o\tau + \phi_y(\tau)\sin \omega_o\tau \tag{3.28}$$

by defining

$$\phi(\tau) = \left\{\phi_x^2(\tau) + \phi_y^2(\tau)\right\}^{\frac{1}{2}} \tag{3.29}$$

and

$$\Lambda(\tau) = \arctan -\frac{\phi_y(\tau)}{\phi_x(\tau)} \tag{3.30}$$

Incorporation of these two definitions into equation (3.27) gives the following expression for the polar co-ordinate version of the joint characteristic function

$$Mp(\alpha_1,\beta_1,\alpha_2,\beta_2) = \exp\left[-\frac{1}{2}\left\{\phi(o)[\alpha_1^2 + \alpha_2^2] + 2\alpha_1\alpha_2\,\phi(\tau)\cos\left[[\beta_1-\beta_2] + \Lambda(\tau)\right]\right\}\right] \tag{3.31}$$

Return now to the original problem of determining the output autocorrelation function and substitute the characteristic function of equation (3.31) into the general expression of equation (3.12). After the appropriate terms are grouped together the autocorrelation function of equation (3.12) can be expressed as

$$\bar{R}(\tau) = -\frac{1}{(2\pi)^2}\exp j\omega_o\tau \iint_0^\infty \alpha_1\alpha_2 \exp\left[-\frac{1}{2}\phi(o)[\alpha_1^2+\alpha_2^2]\right]$$

$$\times \iint_{-\pi}^{\pi} \exp j[\beta_2-\beta_1]\exp\left[j\left\{\alpha_1\alpha_2\ j\phi(\tau)\cos[\beta_1-\beta_2+\Lambda(\tau)]\right\}\right] d\beta_1 d\beta_2$$

$$\times \int_0^\infty \rho_1 J_1(\alpha_1\rho_1)\bar{g}^*(\rho_1)d\rho_1 \int_0^\infty \rho_2 J_1(\alpha_2\rho_2)\bar{g}(\rho_2)d\rho_2 d\alpha_1 d\alpha_2 \qquad (3.32)$$

The integration with respect to $\beta_1$ and $\beta_2$ can now be performed by making use of equation (A.5) in Appendix A and noticing that

$$\iint_{-\pi}^{\pi} \exp\ j[\beta_2-\beta_1]\exp\ j\left\{\alpha_1\alpha_2\ \ j\phi(\tau)\cos[\beta_1-\beta_2+\Lambda(\tau)]\right\}\ \ d\beta_1 d\beta_2 \qquad (3.33)$$

$$= \int_{-\pi}^{\pi} \exp\ -j\beta_1 \int_{-\pi}^{\pi} \exp\left[j\left\{\beta_2-\alpha_1\alpha_2 j\phi(\tau)\cos[\beta_2-(\beta_1+\Lambda(\tau))]\right\}\right] d\beta_1 d\beta_2 \qquad (3.34)$$

$$= \int_{-\pi}^{\pi} 2\pi j\ \exp\ -j\beta_1\ \exp\ +j\beta_1\ \exp\ j\Lambda(\tau)J_1(j\alpha_1\alpha_2\phi(\tau))d\beta_2 \qquad (3.35)$$

$$= (2\pi)^2 j\ \exp[j\Lambda(\tau)]\ J_1(j\alpha_1\alpha_2\phi(\tau)) \qquad (3.36)$$

Conversion of the Bessel function $J_1$ to a modified Bessel function $I_1$ through an application of formula (A.14), allows us to write the complex autocorrelation function of equation (3.32) in the form

$$\bar{R}(\tau) = \exp\ j[\omega_o\tau+\Lambda(\tau)] \iint_0^\infty \alpha_1\alpha_2\ \exp\left\{-\frac{1}{2}\phi(o)[\alpha_1^2+\alpha_2^2]\right\} I_1(\alpha_1\alpha_2\phi(\tau))$$

$$\times \int_0^\infty \rho_1 J_1(\alpha_1\rho_1)\bar{g}^*(\rho_1)d\rho_1 \int_0^\infty \rho_2 J_1(\alpha_2\rho_2)\bar{g}(\rho_2)d\rho_2 d\alpha_1 d\alpha_2 \qquad (3.37)$$

At this point in the development it is possible to make use of the Bessel Function relationship, given by equation (A.6) in Appendix A by

letting $p = 1$, $a = \alpha_1\sqrt{2\phi(\tau)}$ and $\nu = 1$. If this relationship is used the expression for the autocorrelation function given in equation (3.37) reduces to

$$\bar{R}(\tau) = \text{expj}[\omega_o\tau + \Lambda(\tau)] \int_0^\infty 2t\,\text{exp}-t^2 \left| \int_0^\infty \alpha \exp\left\{-\frac{\alpha^2}{2}[\phi(o)-\phi(\tau)]\right\} J_1\left(t\alpha\sqrt{2\phi(\tau)}\right) \right.$$

$$\left. \times \int_0^\infty \rho J_1(\alpha\rho)\bar{g}(\rho)d\rho d\alpha \right|^2 dt \qquad (3.38)$$

At first it may seem that the introduction of another integration variable, t, is a retrograde step but it does lead to an evaluation of the integrals in equation (3.38)

As was discussed in Section (2), the nonlinear characteristic $\bar{g}(\xi)$ will be represented by the complex Fourier-Bessel series expansion of equation (2.32) with $\nu = 1$.

Consider now the integral within the magnitude signs in expression (3.38) and substitute into this expression the series expression (2.32)

$$\int_0^\infty \alpha \exp\left\{-\frac{\alpha^2}{2}[\phi(o)-\phi(\tau)]\right\} J_1\left(t\alpha\sqrt{2\phi(t)}\right) \int_0^\infty \rho J_1(\alpha\rho)\bar{g}(\rho)d\rho d\alpha$$

$$= \sum_{k=1}^\infty \bar{a}_k \int_0^\infty \alpha \exp\left\{-\frac{\alpha^2}{a}[\phi(o) - \phi(\tau)]\right\} J_1\left(t\alpha\sqrt{2\phi(\tau)}\right)$$

$$\times \int_0^\infty \rho J_1(\alpha\rho)\, J_1(\Omega_k\rho)d\alpha d\rho \qquad (3.39)$$

The integrals on the right-hand side of equation (3.39) are in the form of the inversion Hankel's repeated integral, given by equation (A.9) in Appendix A. From equations (A.10) and (A.11) of Appendix A it is obvious that the convergence condition required for the evaluation of Hankel's repeated integral, given by equation (A.7) is satisfied by the right-hand side of equation (3.39) and thus the autocorrelation function of equation (3.38) becomes

$$\bar{R}(\tau) = \exp j\left\{\omega_o \tau + \Lambda(\tau)\right\} \sum_{\ell=1}^{\infty} \sum_{m=1}^{\infty} \bar{a}_m \bar{a}_\ell^* \exp\left\{-\frac{1}{2}(\Omega_m^2 + \Omega_\ell^2)(\phi(o) - \phi(\tau))\right\}$$

$$\times \int_0^{\infty} 2t \exp -t^2 J_1\left\{\Omega_\ell t \sqrt{2\phi(\tau)}\right\} J_1\left\{\Omega_m t \sqrt{2\phi(\tau)}\right\} dt \qquad (3.40)$$

Another use of relationship (A.6) in Appendix A simplifies this expression to give the result

$$\bar{R}(\tau) = \exp j\{\omega_o \tau + \Lambda(\tau)\} \sum_{\ell=1}^{\infty} \sum_{m=1}^{\infty} \bar{a}_m \bar{a}_\ell^* \exp\left\{-\frac{1}{2}\phi(o)(\Omega_\ell^2 + \Omega_m^2)\right\} I_1\left\{\Omega_\ell \Omega_m \phi(\tau)\right\} \qquad (3.41)$$

Examine for the moment the quanity within the summation signs. With the exception of the $\bar{a}_m \bar{a}_\ell^*$ term the expression is symmetrical in m and $\ell$. Consider arranging each term in this double summation as a point in a square matrix in which m is the column number and $\ell$ is the row number. The terms on the principal diagonal are certainly real since $m = \ell$. For each off-diagonal term given by $a_m a_\ell^*$ there is another term $a_m^* a_\ell$. It is easy to demonstrate that $(a_m a_\ell^*)_\ell^* = a_m^* a_\ell$. This means that the double summation in equation (3.41) results in a real term and hence the autocorrelation function of the output signal can be expressed as

$$R_z(\tau) = \cos(\omega_o \tau + \Lambda(\tau)) \sum_{\ell=1}^{\infty} \sum_{m=1}^{\infty} \frac{\bar{a}_m \bar{a}_\ell^*}{2} \exp\left\{-\frac{1}{2}\phi(o)(\Omega_\ell^2 + \Omega_m^2)\right\} I_1\left\{\Omega_\ell \Omega_m \phi(\tau)\right\} \qquad (3.42)$$

It is interesting to observe that this expression is similar in structure to the equivalent expression (equation (33)) derived by Pawula [7] for an error-function limiter with quadratic AM-PM conversion.

Following the analysis technique used by Pawula [7] at this point this output autocorrelation function can be separated into an undistorted replica of the input autocorrelation function (except for a scaling factor) and the intermodulation distortion autocorrelation. This separation is obtained by a use of the series expansion for $I_1(x)$ given by Equation (A.12) given in Appendix A. The desired signal output term is then

$$R_s(\tau) = \phi(\tau)\cos(\omega_o \tau + \Lambda(\tau)) \sum_{\ell=1}^{\infty} \sum_{m=1}^{\infty} \frac{\bar{a}_m \bar{a}_\ell^*}{4} \Omega_\ell \Omega_m \exp\left\{-\frac{1}{2}\phi(o)(\Omega_\ell^2 + \Omega_m^2)\right\} \qquad (3.43)$$

The intermodulation distortion term can now be written as

$$R_D(\tau) = \cos(\omega_o \tau + \Lambda(\tau)) \sum_{\ell=1}^{\infty} \sum_{m=1}^{\infty} \frac{\bar{a}_m \bar{a}_\ell^*}{2} \exp\left\{-\frac{1}{2}\phi(o)\ (\Omega_\ell^2 + \Omega_m^2)\right\}$$

$$\times \left[ I_1\{\Omega_\ell \Omega_m \phi(\tau)\} - \frac{\Omega_\ell \Omega_m}{2} \phi(\tau) \right] \qquad (3.44)$$

An application of the Fast Fourier Transform (FFT) algorithm to the expression obtained in equation (3.44) will give the power spectral density of the intermodulation distortion. This can be normalized to the output signal level by calculating the amplifier gain from equation (3.43).

## 3.2 DISCUSSION

Since the computation time required to perform a FFT computation is independent of the actual signal shape the computation procedure outlined above is generally independent of the number of individual user signals. This of course assumes the total bandwidth is fixed or that the frequency resolution is allowed to vary. The penalty paid is that the composite signal must exhibit gaussian properties.

An examination of equation (3.43) shows that the analysis technique in this section must be used only when weak signal suppression is not significant. The approach of this section does permit computations to be made when the exact analysis of Section (2) becomes too expensive due to excessive computation time.

Although it is possible to write an integral expression for the coefficients of the Bessel-Fourier Series expanison (see Watson [15]), it is more efficient to determine the coefficients through the use of a curve fitting technique. This approach will most likely lead to a more accurate curve fit for a finite series expansion and also permit the parameters $\{\Omega_k\}$ to be general. The curve fitting can be efficiently performed by the use of a pattern search technique described by Wilde and Beightler [19] and a mean-squared-error index of performance.

Before the curve fitting operation it is usually benefical to normalize the actual amplifier characteristic so that "saturation" occurs when $\rho \gtrsim 1$. The curve fit is then usually performed over some finite region R in which the amplifier saturates when $\rho \gtrsim 1$.

It was observed by Kaye, George and Eric [13] that in order to obtain a good curve fit over some region of interest R and avoid the problem of zeros of the expansion terms at the boundary of this region R, it is necessary to perform the curve fit over an extended region $R^1$. An analysis of a normal distribution function shows that there is less than a 1% probability of the signal peak power exceeding a level 9 dB greater than the mean signal power. Conversion of this to a voltage amplitude scale shows that, if R' = 3R and the mean signal power at the output to the transponder is at the limit of the range of interest, then there is less than a 1% probability that signal peaks will occur outside of this region. Thus, if R represents the maximum voltage of interest the curve fit should be performed over a region R' where $R' \gtrsim 3R$.

It has also been determined that the Bessel function zeros, $\Omega_k$, can be approximated by

$$\Omega_k \approx (2k-1)\pi \tag{3.45}$$

with no significant effect on the quality of representation of the amplifier characteristics. If the approximation of equation (3.45) is used, the coefficients of the Fourier-Bessel series expansion become the coefficients of a Fourier-sine expansion of the amplifier's instantaneous voltage transfer function.

Notice that equations (3.43) and (3.44) permit the individual user signals to be either modulated signals or sinusoidal carriers. The autocorrelation function $\phi(\tau)$ can be determined analytically or by a FFT operation on the signal power spectrum, which ever is more convenient. In the evaluation of these two expressions it is evident that the double summation need only be performed over one half of the matrix of terms because the complex conjugate of the summation performed in this manner is identical to equation (3.44).

Lastly, it is interesting to observe that it is possible to start with the equation for the characteristic function of a gaussian process, assume sinusoidal user signals and the analysis of this section results in the final equations of Section 2. Thus, even though a gaussian composite signal is assumed, the more general equations of Section 2 result. This development is contained in Appendix B.

# 4. PREDICTION OF INTERMODULATION NOISE

The purpose of this section is to describe some results of the use of the analysis of Sections 2 and 3. Before doing this the computer programs which have been developed will be briefly described.

## 4.1 COMPUTER PROGRAMS

Computer programs have been developed to perform the following:

1. model an amplifier by a complex Fourier-Bessel series expansion, (as per equation (2.32))

2. perform a sinusoidal intermodulation noise analysis as per the approach of Section 2, (equation (2.36) & (2.37))

3. perform a gaussian intermodulation analysis for the following signal types: (equation (3.43) & (3.44))

   (a) gaussian spectral shape,

   (b) sum of regions of constant power spectral density,

   (c) sum of sinusoids,

   (d) sum of binary modulated PSK and/or FSK signals.

The first two programs will be discussed in Section 5. It suffices to say at this point that up to and including a 20-term complex Fourier-Bessel series expansion can be generated by the first program while the second program can be useful in the analysis of up to approximately ten carriers. The exact computer time is a function of the number of terms in the expansion.

The third program is in reality several programs. There is a main nonlinear analysis subroutine which is common to all of the programs. The difference being that programs use different signal spectrum generation subroutines. To check the operation of the computer programs and the analysis approach, outlined in Section 3, an erf function amplifier characteristic was analysed for signals with a gaussian and rectangular power spectral shapes. The results are shown in Figures 2 to 4.

In Figure 2 the signal-to-intermod (S/IM) ratio at the centre of the band is plotted against the input signal power backoff. The amplifier modeled has an instantaneous voltage characteristic given by

$$Z = \text{erf}(3x) \tag{4.1}$$

where

$$x = A\cos\theta \tag{4.2}$$

Appropriate scaling of values has been performed so that a comparison can be made with the work of Pawula et al. [6] and the analysis of Kaye et al. [12]. As shown in Figure 2, agreement is very good for both the rectangular and gaussian spectrally-shaped signals. It is interesting to notice also that an analysis of 50 carriers by program 3(c) yields results for the worst S/IM ratio (shown in Figure 2) which are in complete agreement with predictions from program 3(b) for a rectangular spectral region. This is as would be expected. For reference purposes the two-carrier-3rd-order S/IM ratio is plotted in Figure 2.

From Figure 3 it is evident that excellent agreement exists between the predictions of Kaye et al. [12] and output signal backoff values calculated by the programs described herein.

The final graph, Figure 4 illustrates the power spectral densities at the amplifier's output for the two signal types. In both cases the input is backed off 10 dB (which corresponds to a 3 dB output backoff). The gaussian shaped power spectra agree with curves published by Pawula et al. [6].

Thus, the main nonlinear analysis subroutine, implementing the analysis of Section 3, results in predictions which are consistent with the work of previous researchers.

## 4.2 TWT AMPLIFIERS

Performance predictions are presented in this section for a Hughes 1177H03 travelling-wave-tube amplifier. The purpose of the graphs of this section is to permit the reader to compare the performance characteristics of TWT amplifiers and class C, solid state amplifiers to be discussed in Section 5.

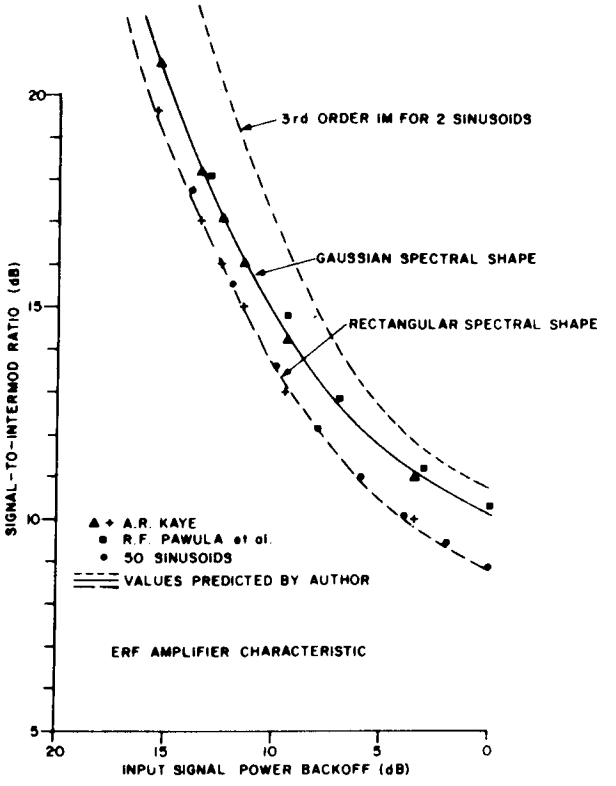


*Figure 2. Signal-to-Noise Power Spectral Density Ratio*

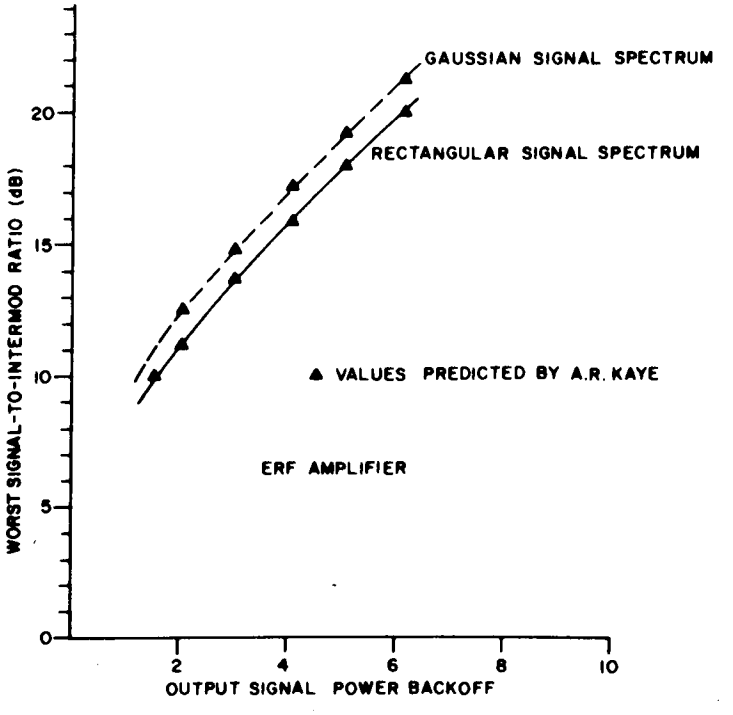


*Figure 3. Signal-to-Intermod Ratio Versus Output Backoff*

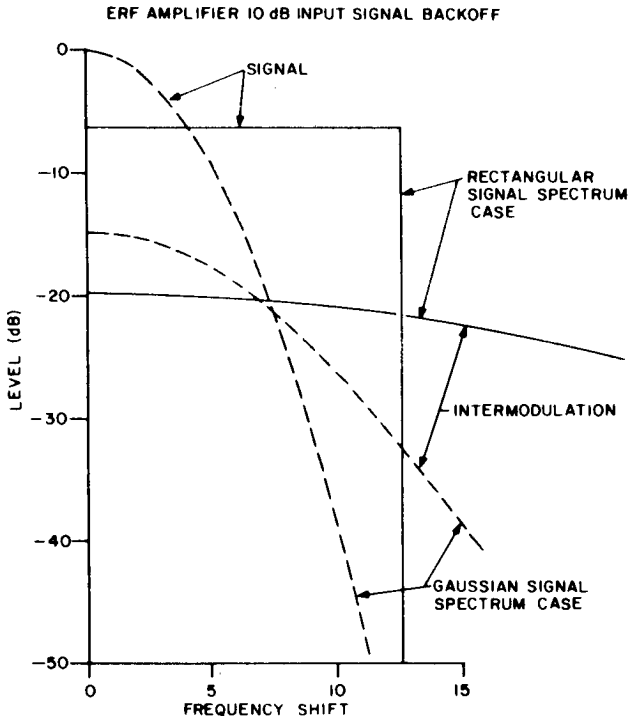


*Figure 4. Power Spectra*

The transfer characteristics of this amplifier are shown in Figure 5. These graphs should be compared with those in Figures 18 and 19. Points of interest are:

1. the TWT amplifier saturates on output power as opposed to the C2M60 amplifier which does not,

2. the TWT amplifier approximates a linear amplifier for large input-backoff values,

3. the phase characteristic is smoother for the TWT,

4. the amplifier gain is considerably greater than that of a single-stage UHF transistor amplifier.

The next graph, Figure 6, illustrates the two-carrier intermodulation performance of this amplifier. The measured performance values are from Eric [3]. Eric shows similar agreement between prediction and measurement.

The multiple carrier intermodulation performance is presented in Figure 7. It is assumed all carriers are at the same power level and are located adjacent one with a constant spacing. The worst signal-to-intermodulation ratio occurs at the centre of the band. Notice that the intermodulation noise continues to decrease with increasing input signal backoff, that is, the amplifier approximates a linear amplifier at large backoff values.

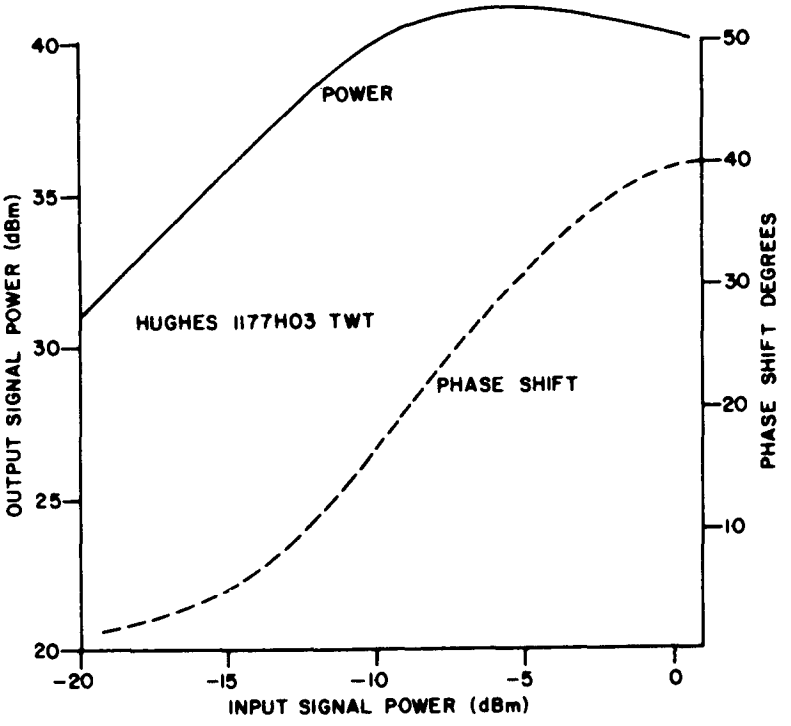


*Figure 5. TWT Transfer Characteristics*

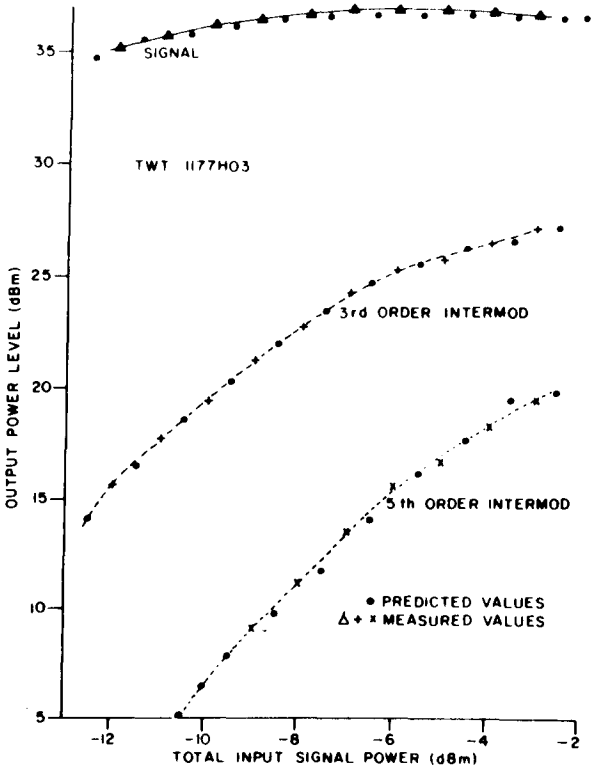


*Figure 6. Two Carrier TWT Performance*

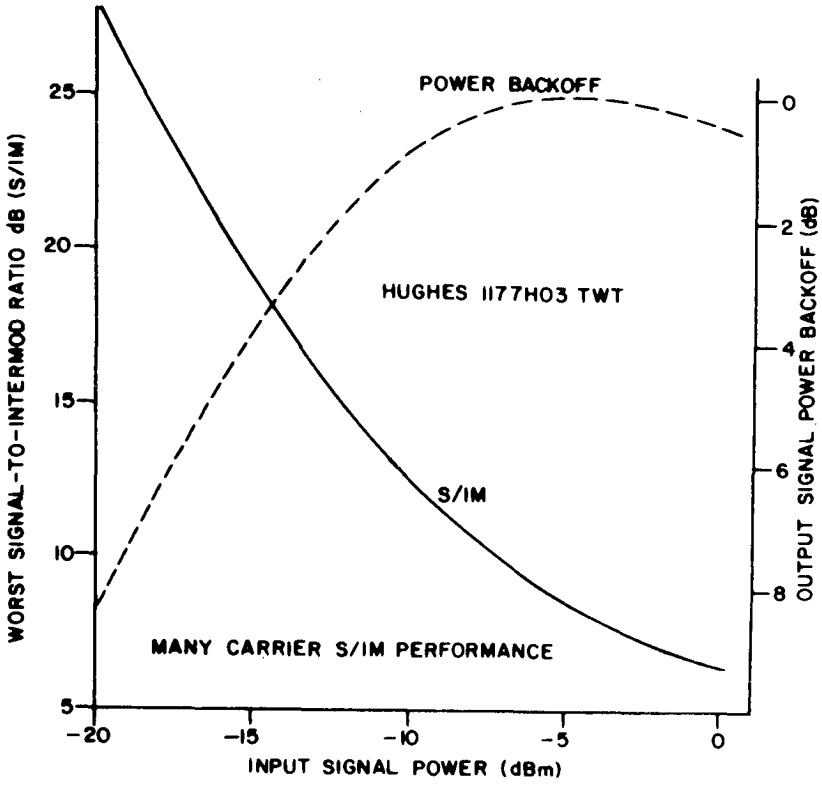


*Figure 7. Many Carrier TWT Performance*

Because of the saturating power transfer characteristic for the TWT, the output signal backoff curve saturates. The maximum output signal power is achieved at an input drive of approximately - 5 dBm.

As is typical of TWT amplifiers, weak signals can be suppressed by strong signals. The severity of this problem is shown in Figure 8. The situation modeled might represent a CW jamming signal trying to gain control of the transponder. To avoid the possibility of significant signal suppression it is necessary to operate the amplifier with an input signal level of less than - 15 dBm.

Similar results are presented in the next section for a C2M60 solid state UHF amplifier.

## 5. SOLID STATE AMPLIFIERS

Before the equations of Section 2 and 3 can be used it is necessary to experimentally measure the nonlinear characteristics of the amplifiers under consideration. The amplifiers of primary concern in this report are solid state UHF power amplifiers of the type which might be considered for use in a UHF satellite transponder.

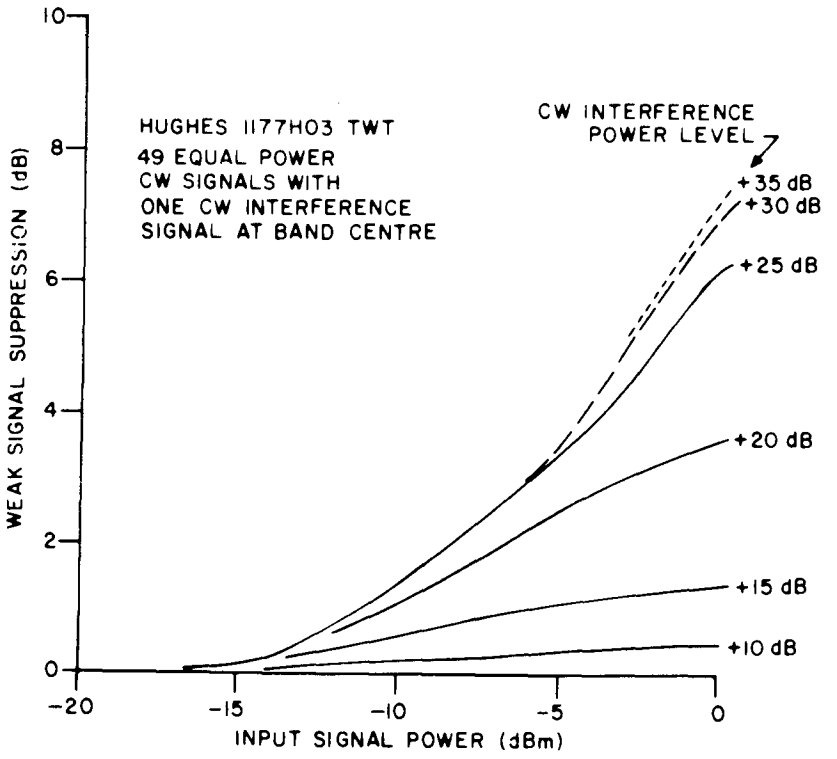


*Figure 8. TWT Signal Suppression*

In this section, a dynamic characteristic measurement technique, as well as, the degree of agreement between measured and predicted two and four carrier intermodulation distortion is discussed. It is demonstrated that when solid state UHF amplifiers are under consideration, a dynamic characteristic measurement test must be performed.

## 5.1 MEASUREMENT TECHNIQUES

The technique conventionally used to measure the transfer characteristic of an amplifier is to insert a sinusoid of a given power level and then record the output power level and the phase relationship of the output sinusoid to the input sinusoid. The input power level is stepped to another value and thus a complete transfer characteristic can be determined. This technique will be referred to as a static measurement.

A static characteristic of a C2M60 transistor amplifier can be measured and the analytical analysis of Section 2 performed. The predicted two-carrier, third-order intermodulation distortion is presented in Figure 9 by the curve labelled "static model". A comparison of this curve with the illustrated measured third-order intermodulation levels, shows a discrepancy of up to 4.5 dB in the best operating region for this amplifier. Notwithstanding this discrepancy, the predicted curve does show an increase in intermodulation distortion at high input power levels due to a saturating effect as well as a high distortion level at low drive levels due to the class-C amplifier "turn-on" characteristic. It is suggested that the

discrepancy of 4.5 dB (around the optimum operating region) is a result of a heating effect within the amplifier; that is, the single sinusoid test signal at high input power levels causes the operating temperature of the amplifier, and hence its characteristics, to change. This is in contrast to a travelling-wave-tube type of amplifier which tends to maintain its operating temperature, regardless of the input signal power.

In order to test this hypothesis the dynamic characteristic measurement technique of Figure 10 was devised. The basic idea is to insert a pulsed amplitude-modulated signal of a low duty cycle into the test amplifier and then with the aid of a network analyzer compare the input signal at any instant in time, with the output signal to determine the amplifier gain and phase shift. The pulse shape used was an amplitude ramp. The "Z" axis bright-up pulse permits a marker to be positioned on the gain and phase characteristic displayed on the network analyzer. This pulse is also used to trigger a peak power reading meter which can be connected to either $I_1$ or $I_2$. Thus the displayed characteristics can be calibrated. Use of this measurement arrangement and a low duty cycle amplitude-modulated signal permits a cool dynamic model of the amplifier to be determined.

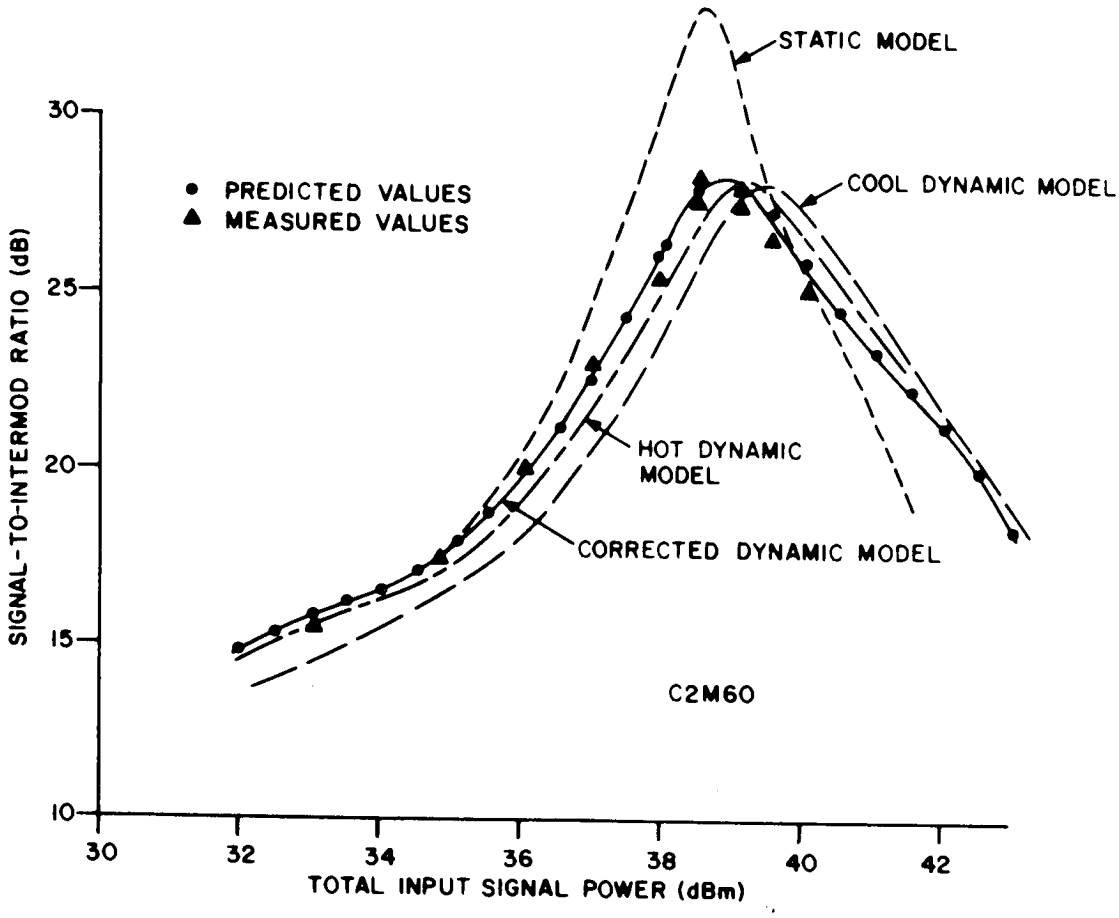


*Figure 9. 3rd Order-Two-Carrier Intermodulation Level*

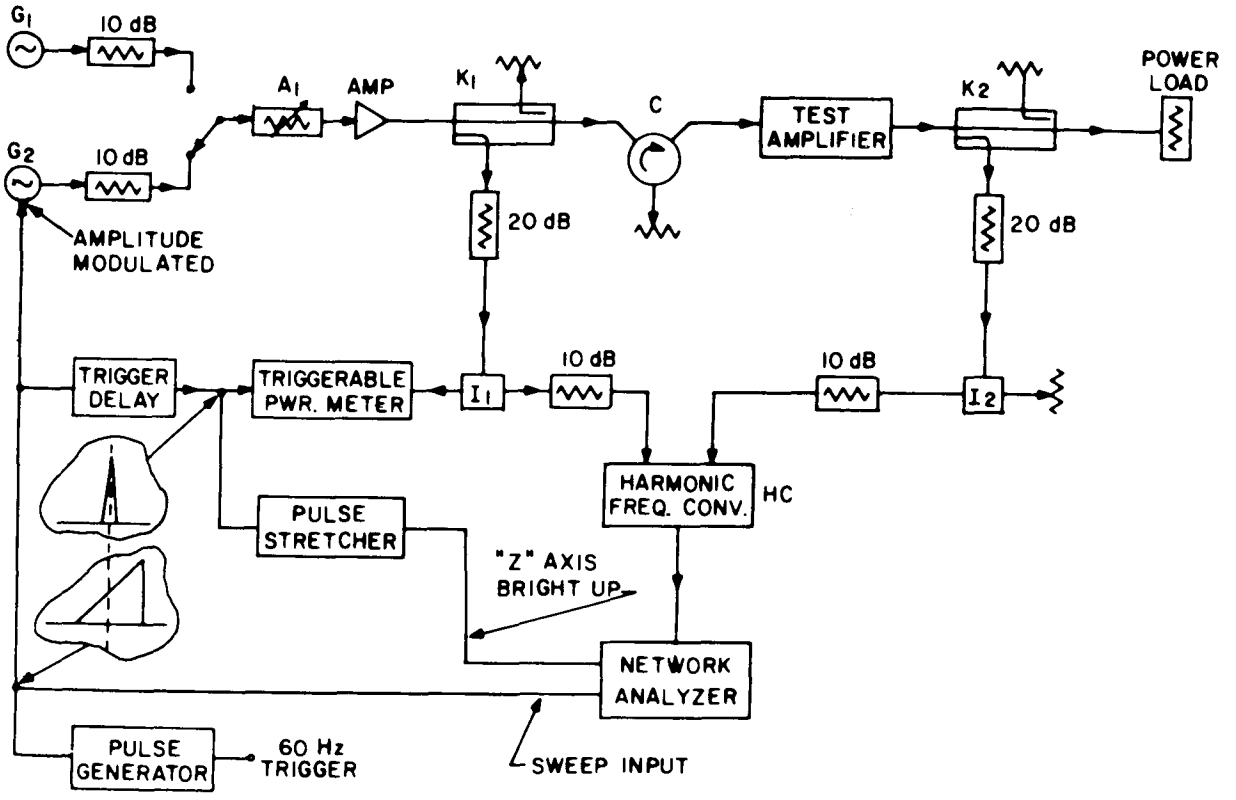


*Figure 10. Dynamic Measurement*

The subsequent predicted third-order two-carrier signal-to-intermodulation distortion ratio is illustrated in Figure 9. Examination of this curve shows that there has been a significant improvement in the shape of the curve although it still appears to be displaced approximately 0.5 dB to the right of the experimentally measured data points.

Since it appears that the amplifier's characteristic is sensitive to temperature it was decided to try to measure the characteristics with the amplifier amplifying a signal at approximately the optimum operating power level. To measure the characteristic dynamically with an actual input signal is difficult since it would require very careful control of the duty cycle and modulation index of the test signal. In order to avoid these difficulties the following approach was used. With reference to Figure 10, a high-powered sinusoid from generator $G_1$ was inserted into the amplifier and allowed to remain there until the test amplifier's temperature has stablized at which time the dynamic test signal from generator $G_2$ was switched to. The switching was performed with a coaxial relay switch so that from the thermal point of view, the switching time can be ignored. As the temperature of the amplifier cooled, changes in the characteristics could be observed on the network analyzer. This change in the gain and phase characteristics was recorded photographically with the aid of a time exposure as illustrated in Figure 11. From these graphs it is possible to develop a "hot dynamic model" for the amplifier which results in the third-order two-carrier-intermodulation performance prediction represented by the hot dynamic model in Figure 9. This

curve is within 0.25 dB of the measured performance. This is within the tolerance of errors and can be corrected for by a change in the normalization constant used by the amplifier modeling program. Thus, the corrected dynamic model results. As illustrated in Figure 9, there is very good agreement between measurement and predictions based upon this model.

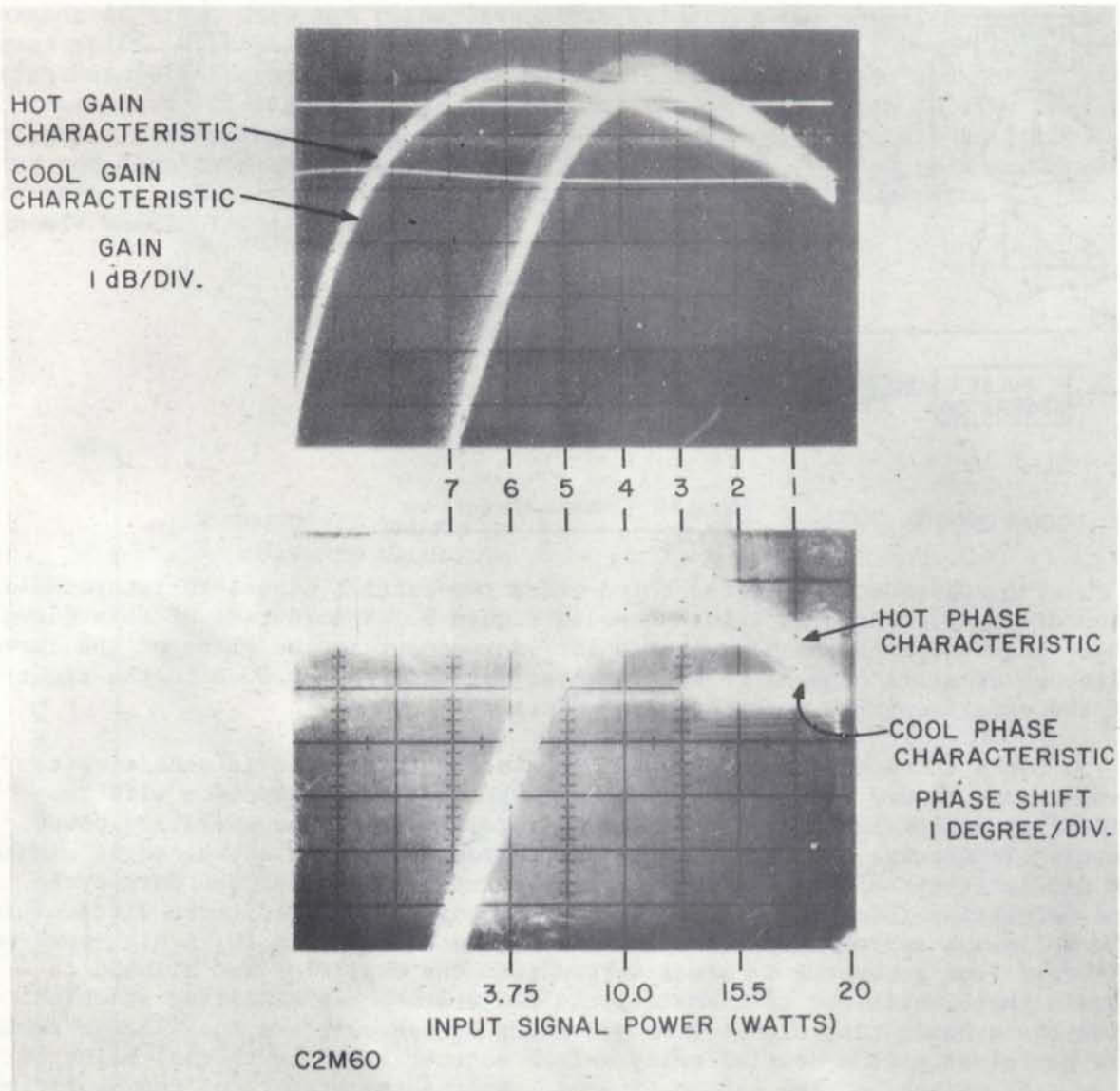


*Figure 11. Dynamic Characteristic*

The agreement for 5th and 7th-order components is illustrated in Figure 12. Superimposed on this graph is the 3rd-order intermodulation performance. Notice that over the operating region of 37 dBm to 40 dBm the 5th-order intermodulation components are dominant. The minimum two-carrier, carrier-to-intermod ratio curve is shown in Figure 13 and illustrates this region of 5th-order intermodulation dominance. The output power spectrum at a 39 dBm input drive level has the appearance shown in Figure 14. This phenomenon of lower 3rd-order components is not observed with class-A travelling-wave-tube amplifiers. It is suggested that this phenomenon is a result of the interaction of a saturating nonlinearity with the class-C "turn-on" region nonlinearity.

Thus, based upon a two-sinusoidal-carrier analysis, the dynamic method of characteristic measurement appears to result in a mathematical model which yields predicted performance in close agreement with measured performance. The measurement and modeling process will be now discussed in more detail.

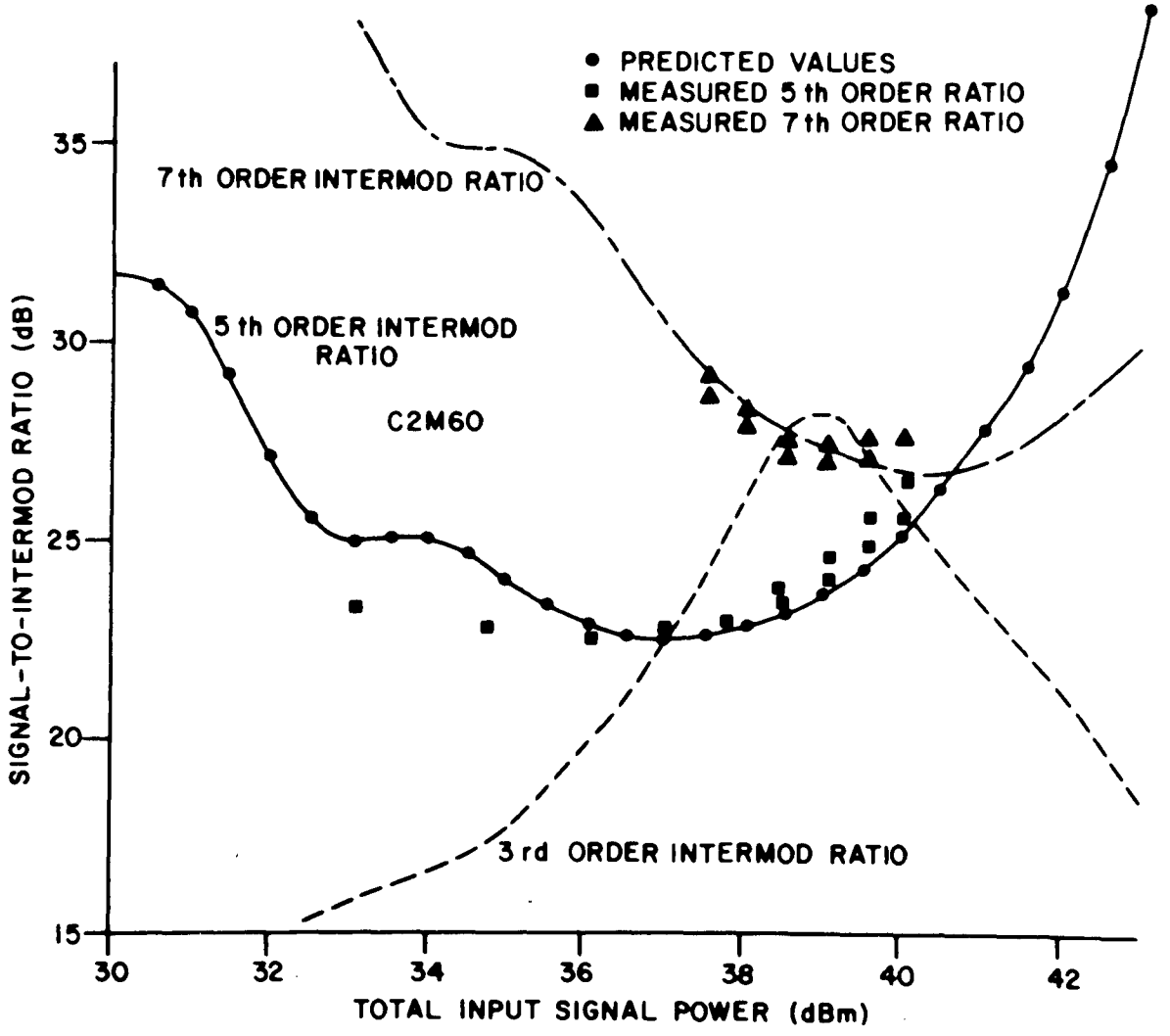


*Figure 12. 5th and 7th Order IM Performance*

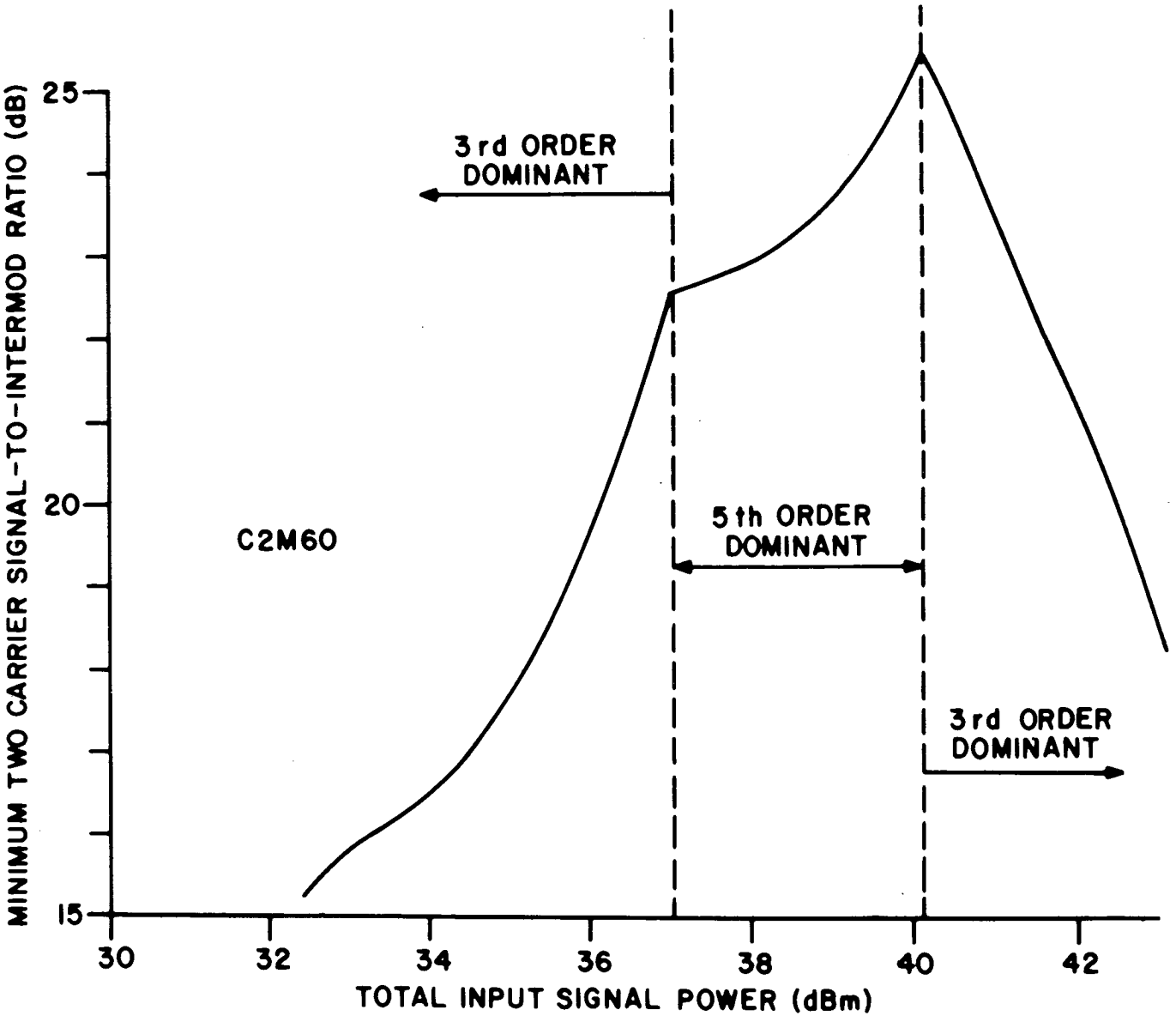


*Figure 13. Minimum Signal-to-Intermod Ratio*

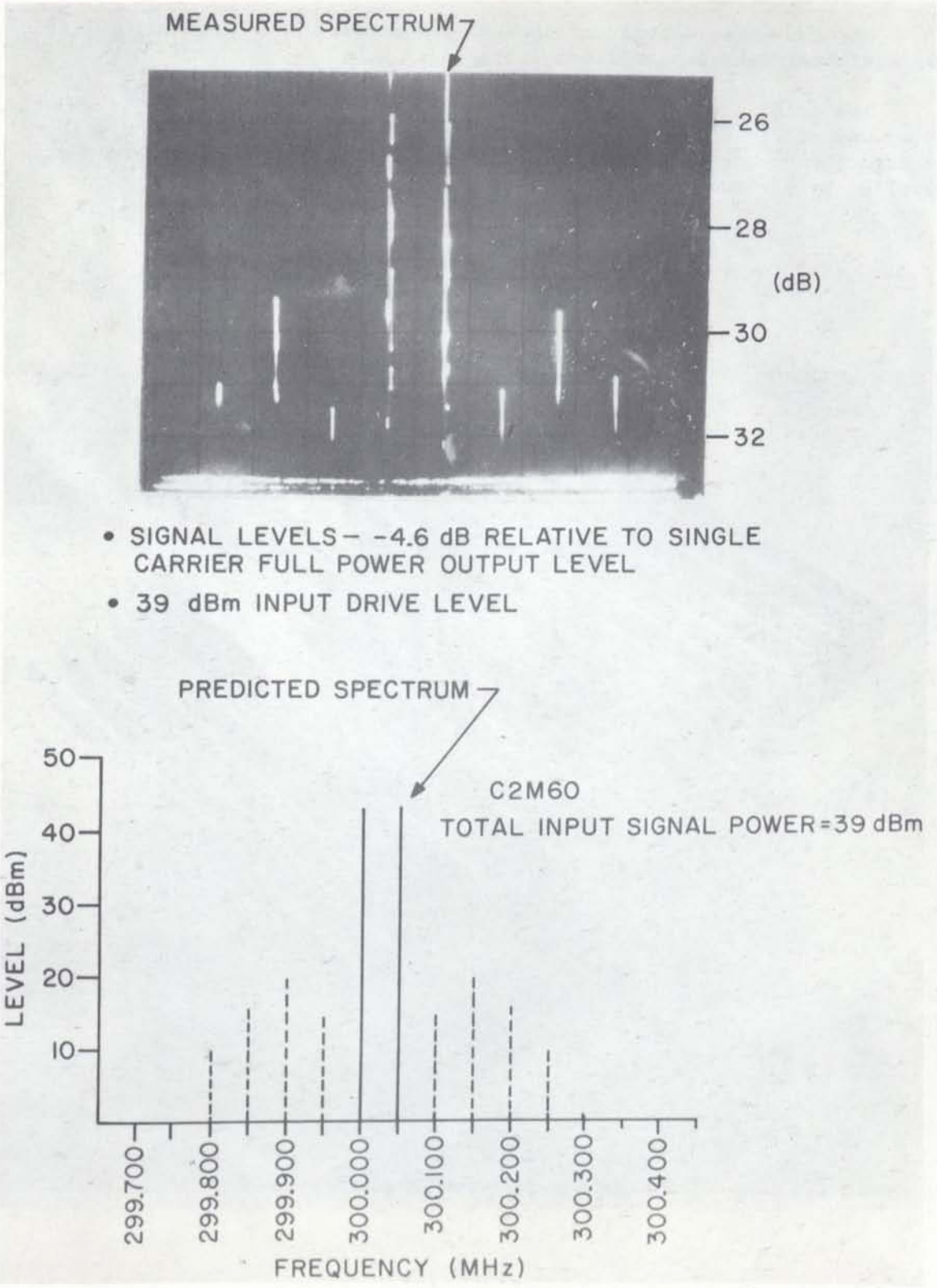


*Figure 14. Two Carrier IM Spectrum*

## 5.2 DYNAMIC MODELING TECHNIQUE

For the experimental arrangement illustrated in Figure 10, a list of the equipment used is contained in Appendix C.

The actual test amplifier is shown in Figures 15 to 17. The mounting shown was one of convenience with no attempt made to design an efficient package for the transistor. As shown in Photo 15, amplifier cooling was supplied by air cooling fins.

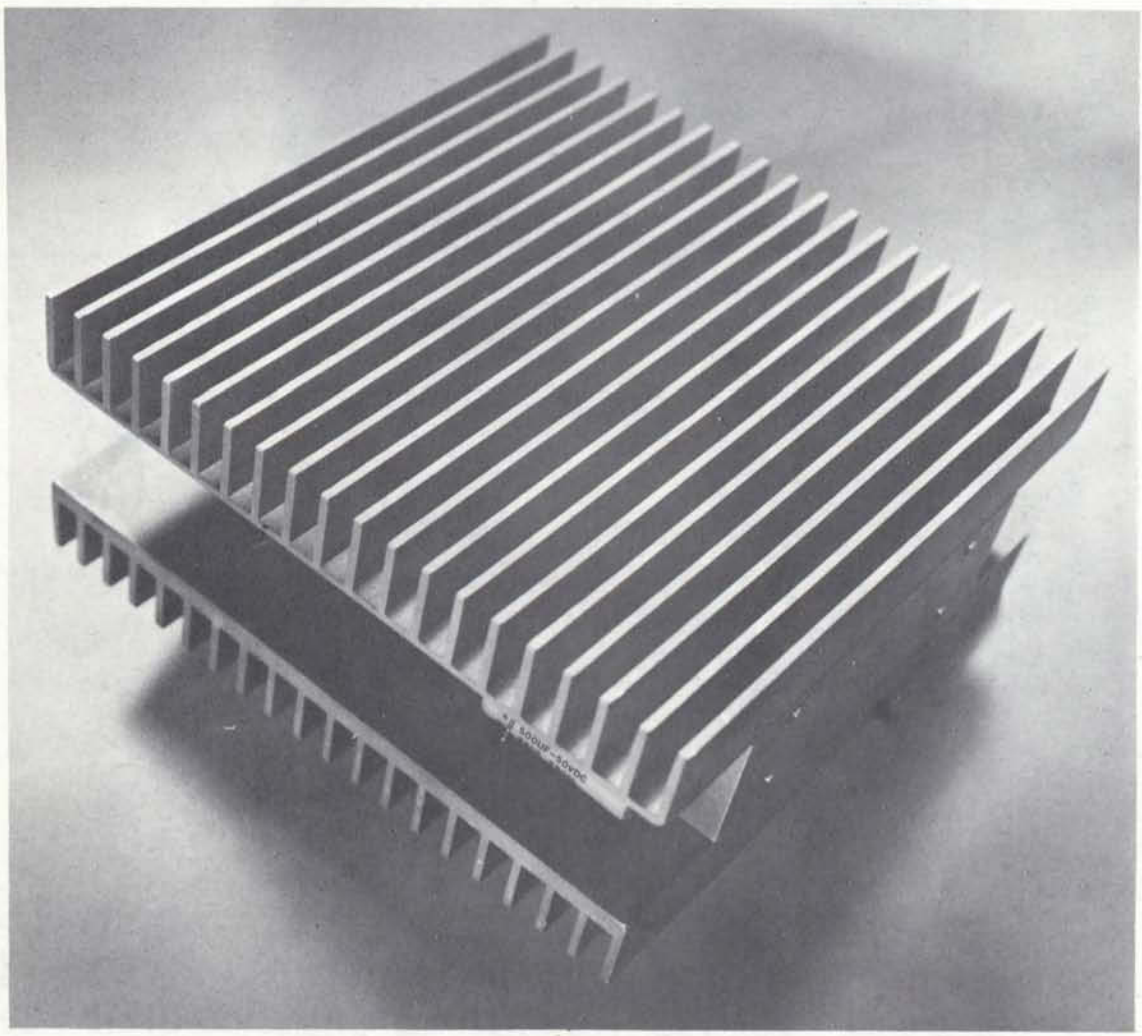

*Figure 15. Test Amplifier Cooling*

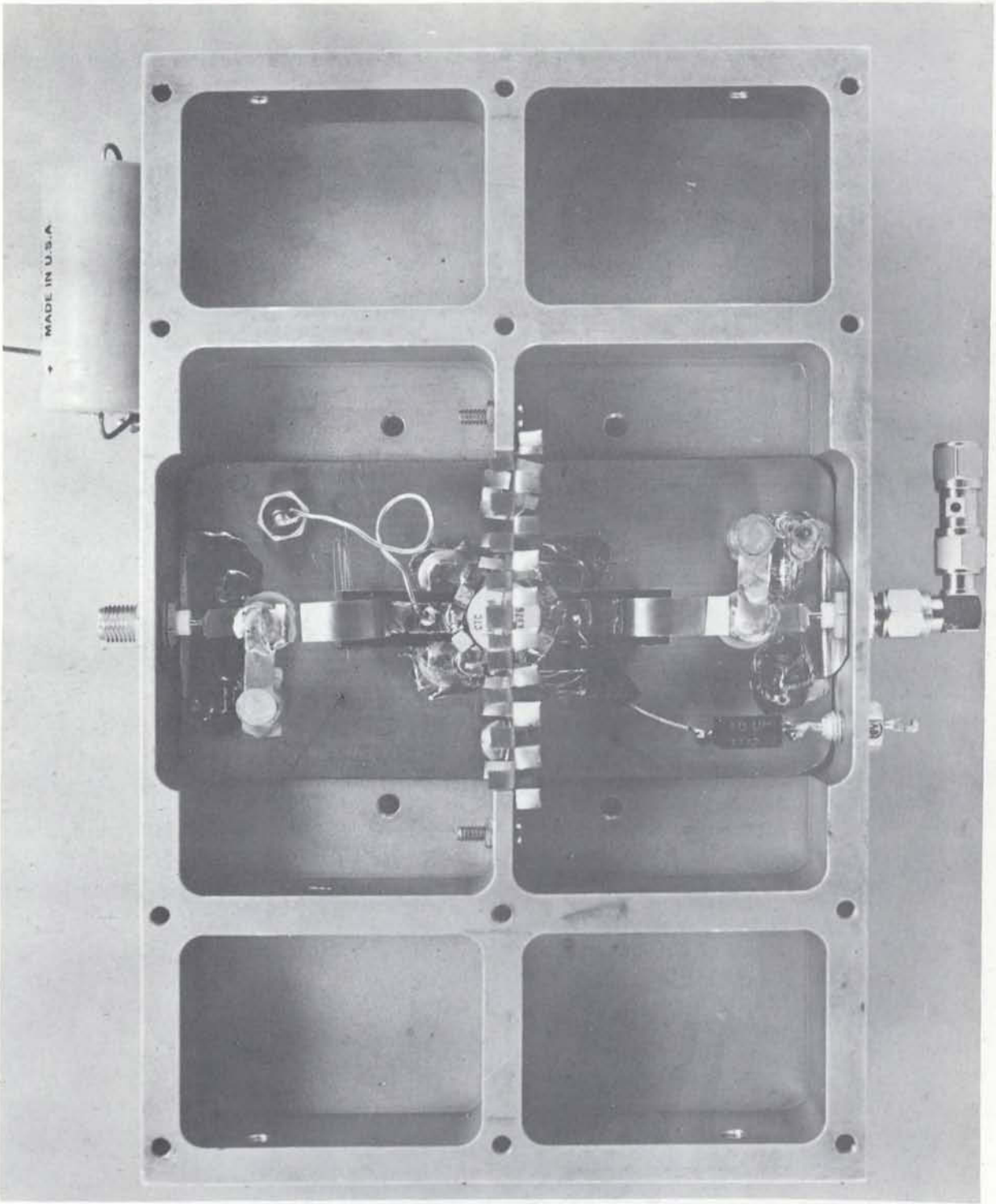


*Figure 16. Component Arrangement*

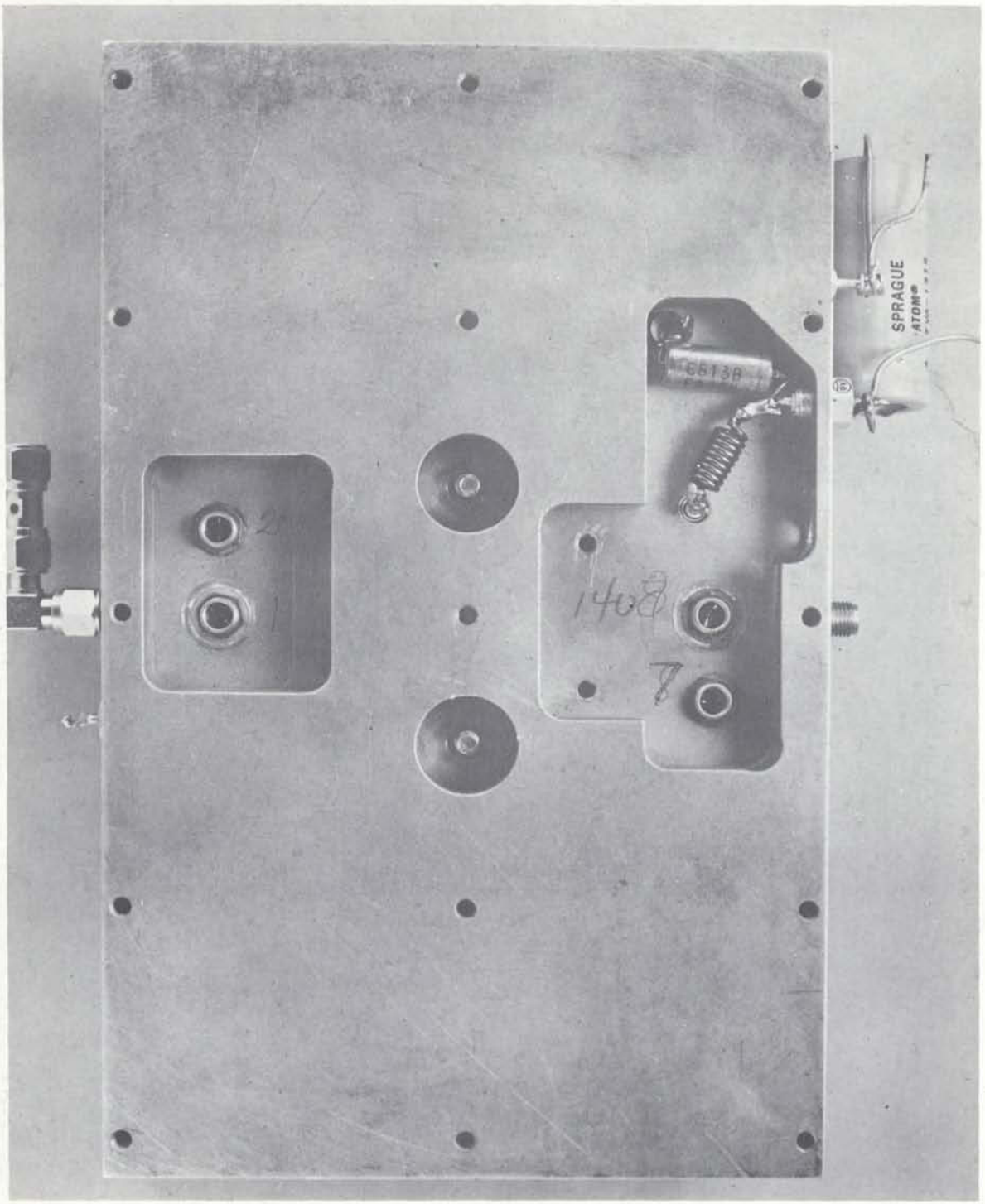


*Figure 17. Test Amplifier Reverse Side*

The basic idea of the dynamic measurement procedure is that an amplitude modulated signal is used to vary the instantaneous input signal power supplied to the test amplifier. The output signal is compared to the input signal and the gain and phase shift versus input signal power are displayed on a network analyzer. The actual power transfer characteristic is measured with the aid of the triggerable peak-power-reading meter. The "Z" axis bright-up pulse indicates to the experimenter where on the amplifier's characteristic a measurement is being made. Either the input or the output instantaneous power is measured depending upon whether the meter M is connected to either $I_1$ or $I_2$. Since this power meter will measure only the power level at its terminals, it is necessary to calibrate the experimental arrangement in order that the power at the test amplifier's terminals can be determined. This calibration can be performed by removing the test amplifier and inserting another precision power meter at the test amplifier's location. Power readings can be made at both the test amplifier's location, as well as, at the peak power reading meter's location. Two calibration factors are thus determined:

1. the first relating the power reading at $I_1$ to the amplifier's input signal power (42.7 dB),

2. the second relating the power measured at $I_2$ to the amplifier's output power (43.0 dB).

---

At this point it must be emphasized that extreme care must be taken in determining these numbers since an error as small as 0.25 dB will shift the amplifier's apparent transfer characteristic.

An amplifier's cold dynamic power transfer characteristic can now be measured with the aid of the peak-reading power meter. At the same time the input power axis of the displayed gain-phase characteristics can be calibrated. The signal phase shift at any particular input power drive level can then be measured with the use of the network analyzer. The cold dynamic transfer characteristic for the C2M60 amplifier, measured in this manner, is presented in Table 1.

These characteristics have been used to generate a complex Fourier-Bessel series expansion cold dynamic model for the C2M60 amplifier and the appropriate intermodulation distortion predictions of Figure 9. To obtain a hot dynamic model it is necessary to examine Figure 11 to determine, at each operating point, the change in the amplifier's gain and phase shift characterisitcs. Corrections can then be made to the values in Table 1 to obtain a hot dynamic model for the amplifier. The corrected dynamic model of Figure 9 is achieved by correcting the input power normalization factor (for the computer programs) to allow for the 0.25 dB shift required for the hot dynamic model. Thus, with this corrected model, a useful Fourier-Bessel series expansion model has been obtained for the C2M60 amplifier.

The actual input data for the computer programs are in units of watts and degrees. The data points are scaled from graphs of the amplifier's transfer characteristics, as illustrated in Figures 18 and 19. In order to ensure that a good characteristic fit is obtained it is necessary to supply the computer program with data at more input power levels than are normally

*TABLE 1.*

*C2M60*

*Cold Dynamic Characteristic*

| INPUT POWER dBm | OUTPUT POWER dBm | PHASE SHIFT Degrees |
|---|---|---|
| 43.0 | 49.0 | 24 |
| 42.6 | 48.8 | 24.5 |
| 41.9 | 48.4 | 25.1 |
| 41.4 | 48.2 | 25.3 |
| 41.0 | 48.0 | 25.4 |
| 40.0 | 47.4 | 25.1 |
| 38.9 | 46.6 | 23.7 |
| 37.6 | 45.3 | 21.2 |
| 36.1 | 43.2 | 17.6 |
| 35.1 | 41.9 | 15.8 |
| 33.7 | 39.4 | 12.8 |
| 32.6 | 37.2 | 11.2 |
| 31.7 | 35.4 | 6.0 |
| 30.8 | 33.6 | —— |

measured experimentally. It has been found that additional extrapolated data points are required at both the high and low-power drive levels. The dynamic measurements have an advantage over static measurement because of the extended measurement region (as illustrated in Figures 18 and 19). This is due to the use of a low duty test signal and hence a cooler amplifier operating temperature. The reader should observe from Figure 18 that unlike TWT amplifiers, the C2M60 solid state UHF amplifier does not saturate on output power but only exhibits a saturating tendency. It has been observed with this and other solid state amplifiers (CM75-28, CM75-28R, XB50, V410) that the transistor is destroyed before true saturation occurs.

The computer program does not model the power and phase characteristics directly but generates an inphase and a quadrature, root-mean-square voltage characteristics and then fits a Fourier-Bessel series expansion to each of

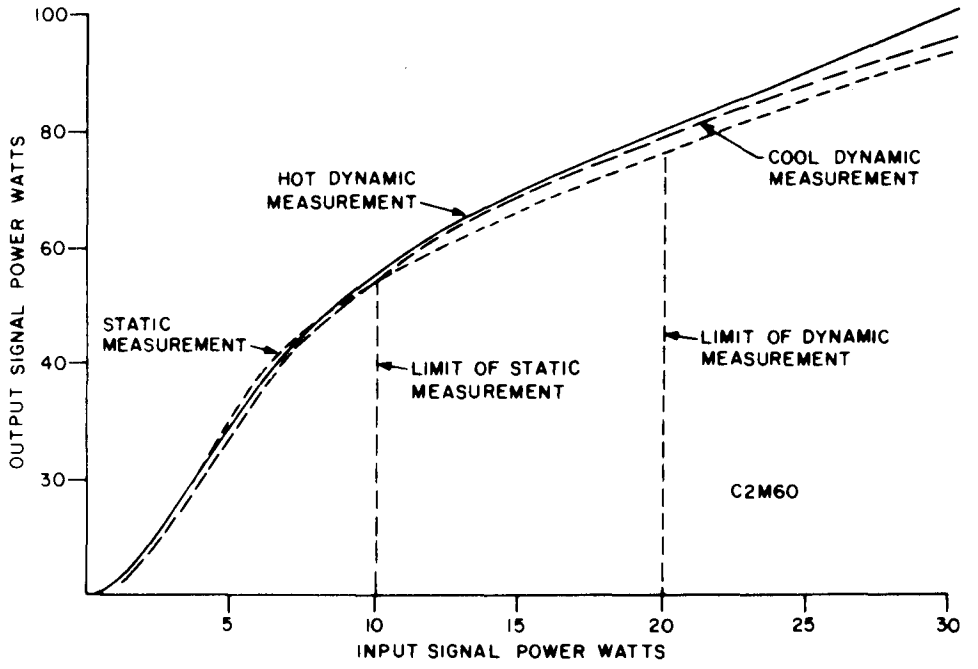


*Figure 18. Amplitude Characteristic*

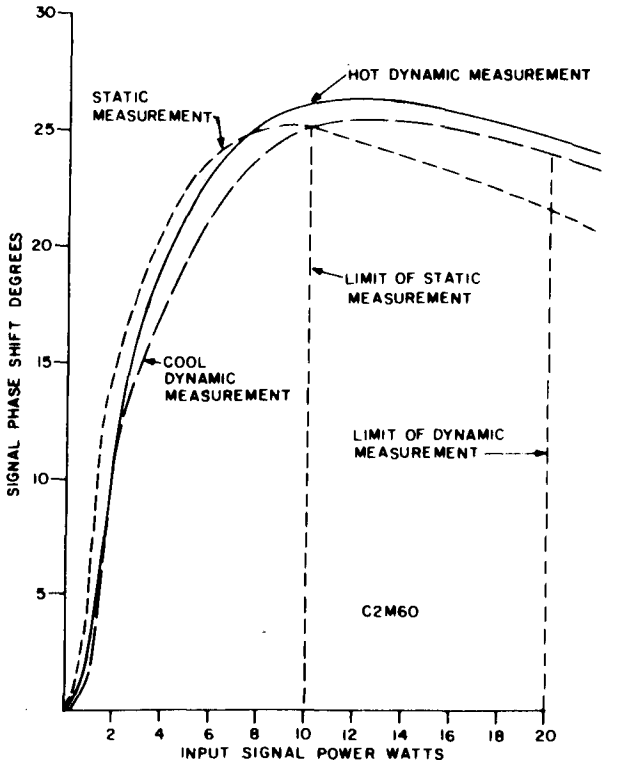


*Figure 19. Phase Characteristic*

these curves. Both of the curves are normalized to input and output power levels supplied by the user. The in-phase coefficients are the real parts of the complex coefficients. The degree of agreement between the predicted (from the expansion) and the measured in-phase and quadrature characteristics indicates the quality of the curve fitting operations. This agreement is demonstrated in Figure 20. The root-mean-square error on the curve fit is usually at least 50 dB below the output power normalization level specified by the user.

From the in-phase and quadrature characteristics it is possible to reconstruct the power and phase characteristics of the amplifier (as shown in Figure 21). Care must be taken in the reconstruction of the phase characteristic at low angles and drive levels since small errors in the component characteristics are magnified through the use of an inverse tangent formula.

The behaviour of the series expansion model over a 60 dB input power range is illustrated in Figure 22. It is generally advisable to examine a graph similar to Figure 22 to ensure the stability of the series expansion in regions immediately exterior to the range of power values of interest.

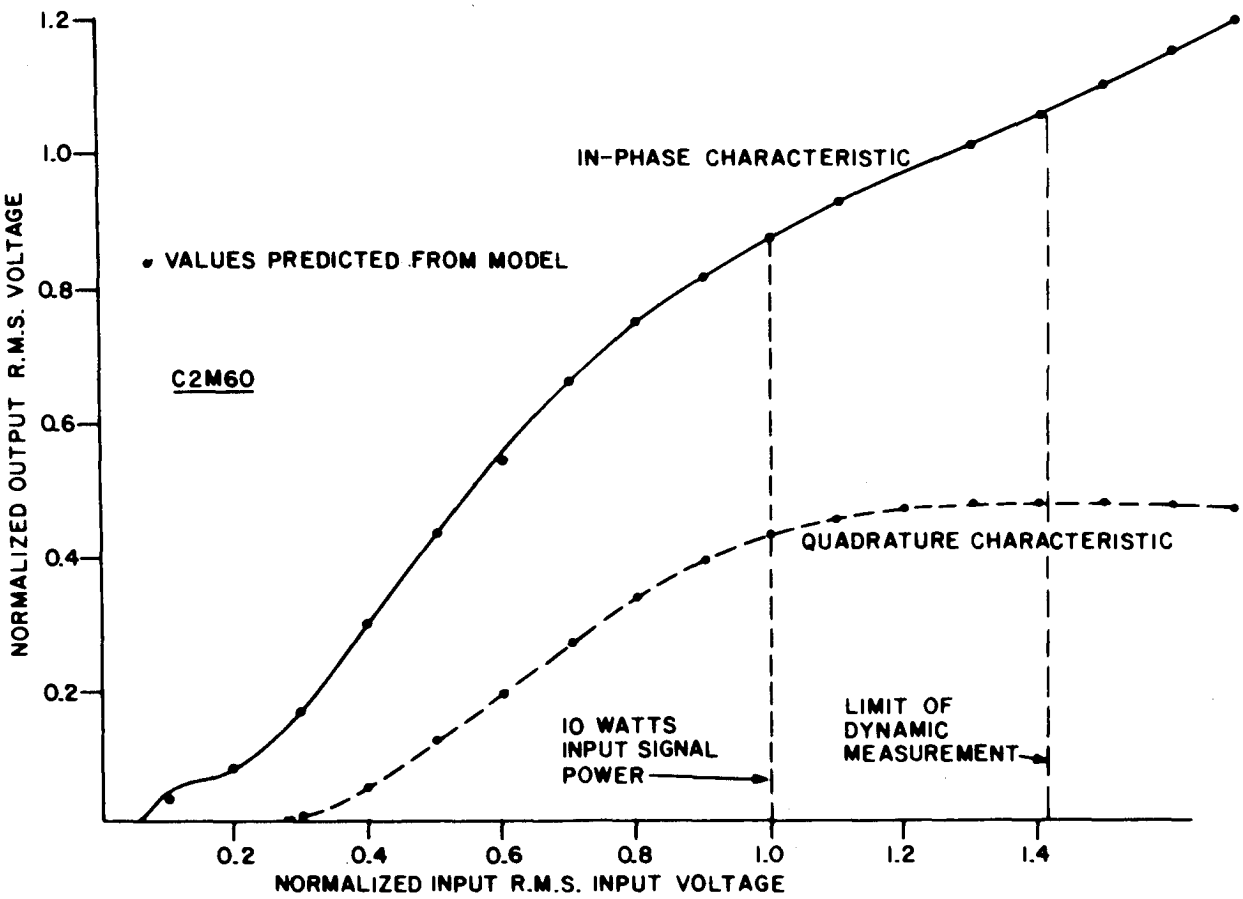


*Figure 20. Component Characteristics*

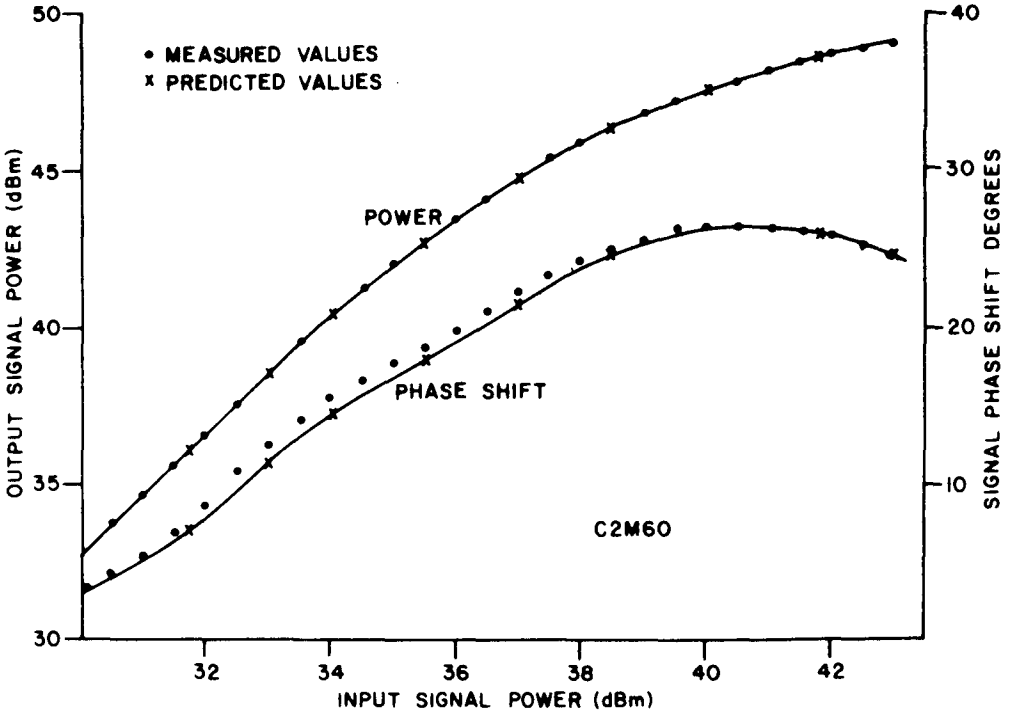


*Figure 21. Reconstructed Characteristic*

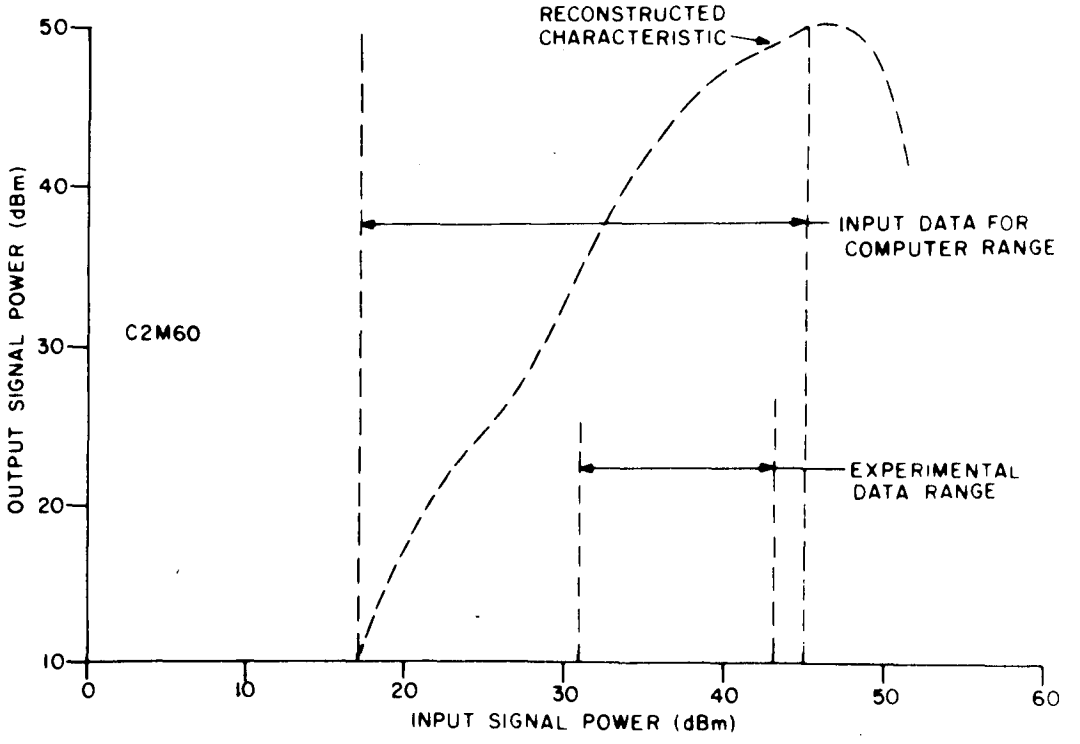


*Figure 22. Extended Characteristic*

## 5.3 MULTICARRIER INTERMODULATION PERFORMANCE

Up to four carrier intermodulation distortion measurements can be performed by the use of the equipment of Figure 23 in the arrangement of Figure 10. The output power spectrum was observed with a spectrum analyzer. The equipment used is listed in Appendix C.

The results of the two-carrier measurements have been presented in Figures 9 to 14. Four-carrier measurements have been made and are compared with predictions in Figures 24 and 25. The measured and predicted output power spectra for the C2M60 amplifier with a 37 dBm input drive are illustrated in Figure 24. It is observed once again that the intermodulation components close to the carrier frequencies are lower than components further away in frequency. A second observation of interest is that the inner two carriers have the highest predicted signal-to-intermodulation distortion power ratio. This is contrary to what is normally achieved with a class-A power saturating amplifier.

A view of intermodulation performance versus input signal drive level is presented in Figure 25. The first sideband components refer to the components adjacent to the carrier frequencies band at 299.950 and 300.200 MHz. The signal-to-intermod ratio used in these graphs is the power ratio of a single carrier to intermodulation distortion level. The signal-to-sideband intermod ratio is the only performance indication which can be readily measured experimentally. From the top graph of Figure 25 it is seen that the agreement between prediction and measurement is good. In any communications system application it is actually the signal-to-intermod ratio, on the carrier frequencies which is of interest. These ratios are presented in the lower graph of Figure 25. Notice that there are two operating points at which all carriers have the same signal-to-intermod ratio.

To complete the set of measurements on this amplifier the two and single-carrier prime power efficiency and single-carrier bandwidth were measured. These curves are presented in Figures 26 and 27 respectively.

The dynamic measurement technique described in this section has been used by Harrison and Moody [20] to predict intermodulation levels for both class-C and class-L (a low intermod mode) amplifiers. Their degree of agreement between measurement and predictions is similar to the agreement shown in this report.

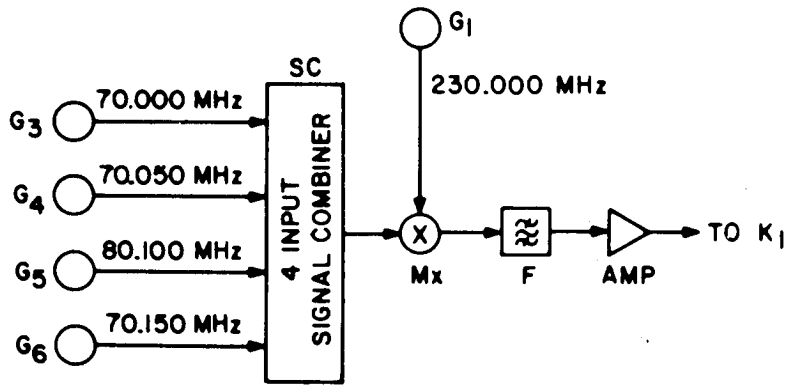


*Figure 23. Four Carrier Equipment*

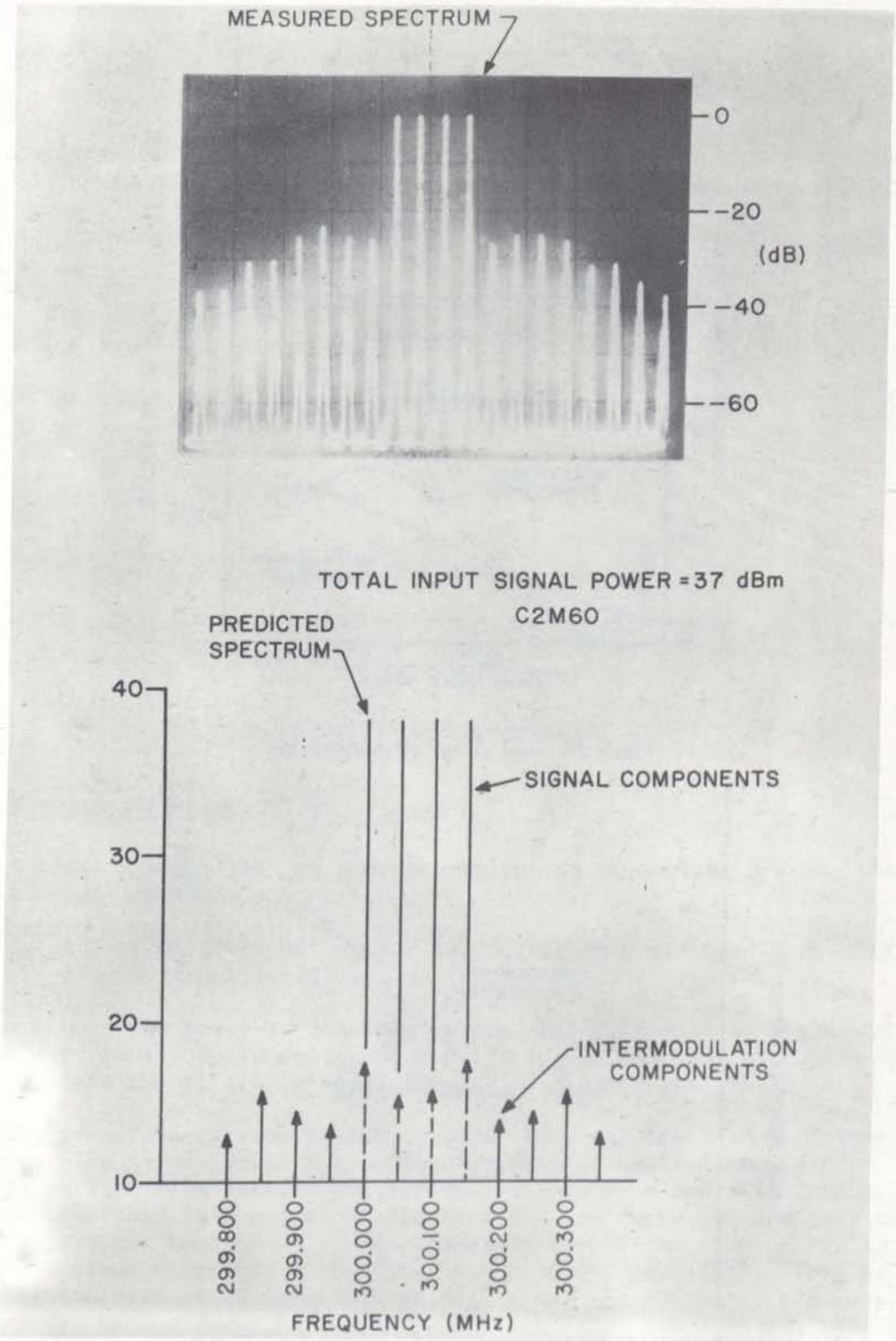


*Figure 24. Four Carrier Spectrum*

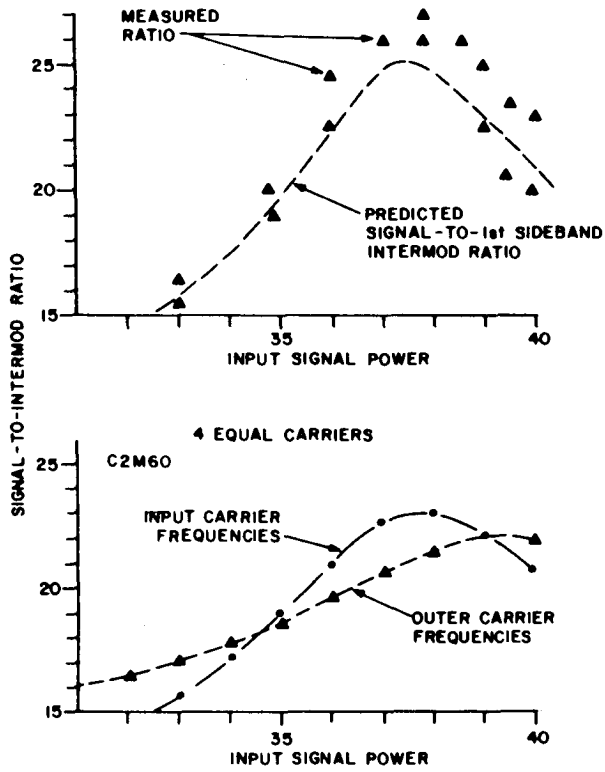


*Figure 25. Four Carrier IM Performance*

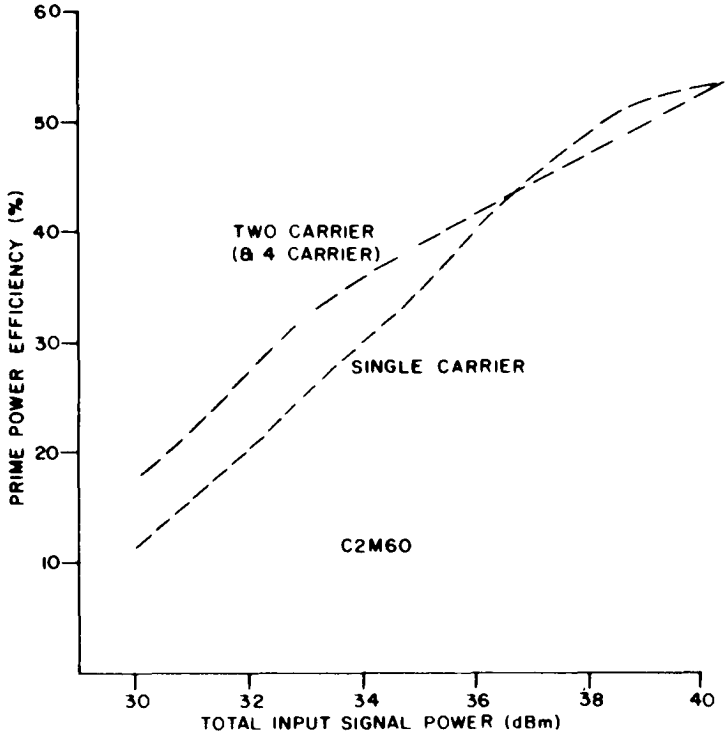


*Figure 26. Prime Power Efficiency*

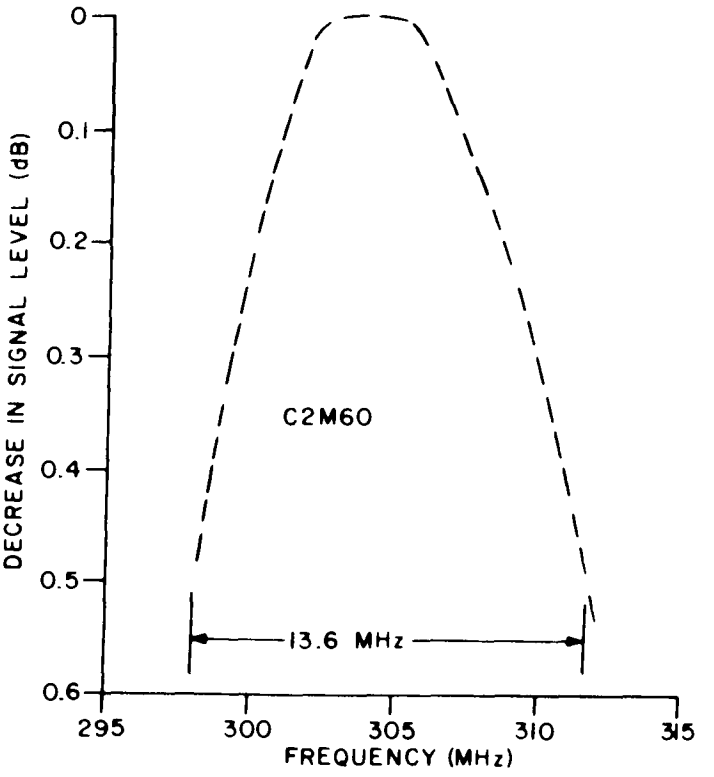


*Figure 27. Amplifier Bandwidth*

## 5.4 UHF SOLID STATE AMPLIFIERS - CLASS C

A class C amplifier has two very important advantages over a linear class A amplifier (TWTs):

1. the prime power efficiency is considerably greater (typically 50-60% versus 10-20%),

2. no prime power is consumed by the amplifier when no signal is present. Solid State UHF amplifiers, of the type discussed in this report are intended for use as Class C amplifiers.

The transfer characteristics, two and four-carrier S/IM performance have been already presented for a C2M60 transistor class C amplifier. The multiple carrier S/IM performance curves for this same amplifier are presented in Figure 28 (this is the dual of Figure 7 for the TWT). In contrast to the TWT it is evident that, from a S/IM performance point of view, there is a definite optimum operating point for the transistor amplifier. This point is in the vicinity of 38 dBm input signal drive. In addition, the output signal power montonically increases with input drive and does not have an optimum input drive for peak output signal power as does the TWT. One very important observation from Figure 28 is that the S/IM performance deteriorates as the transistor is backed-off from a 37 dBm drive level. Thus, it will be necessary if a signal is present to ensure that the input drive to the power

amplifier stage is sufficient so that acceptable S/IM performance is achieved. This is not a problem with a TWT amplifier which backs off into a linear amplifier. This matter is of prime importance in any FDMA demand assignment satellite communication system since the number of individual input signals continually varies.

From the curves of Figure 29 the degree of weak signal suppression to be expected with this type of amplifier is indicated. A comparison with Figure 8 shows the suppression to be less severe than with the previous TWT amplifier. In addition, at low input signal drive levels, the weaker signals gain more than their fair share of the output signal power, that is, signal enhancement occurs. It is interesting to observe that little or no suppression occurs in the optimum operating region of minimum intermodulation noise (i.e., 37 - 39 dBm drive). This latter point could be quite important in anti-jamming considerations of satellite communication systems. Thus, the region of best S/IM performance and high output signal power level is also the operating region where little or no weak-signal suppression occurs.

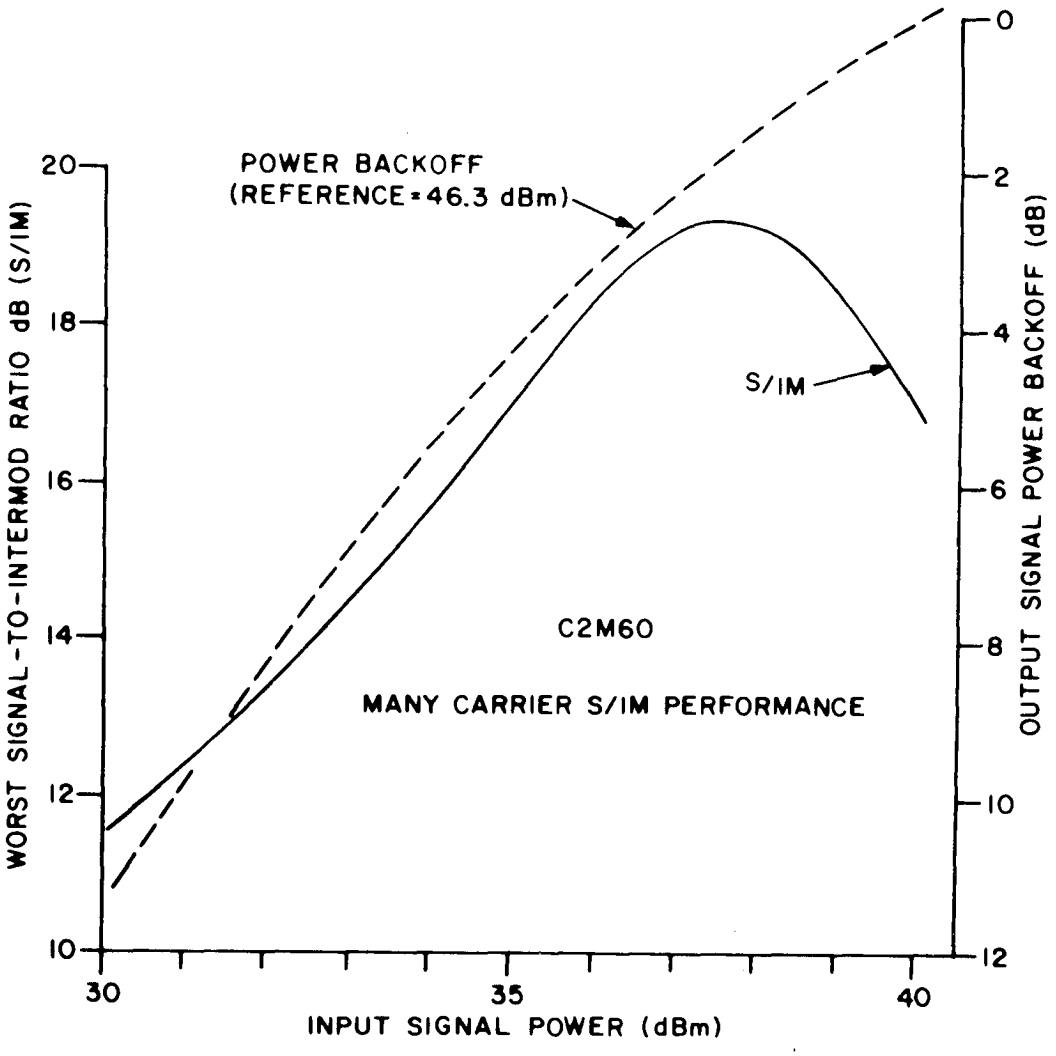


*Figure 28. Many Carrier S/IM Performance*

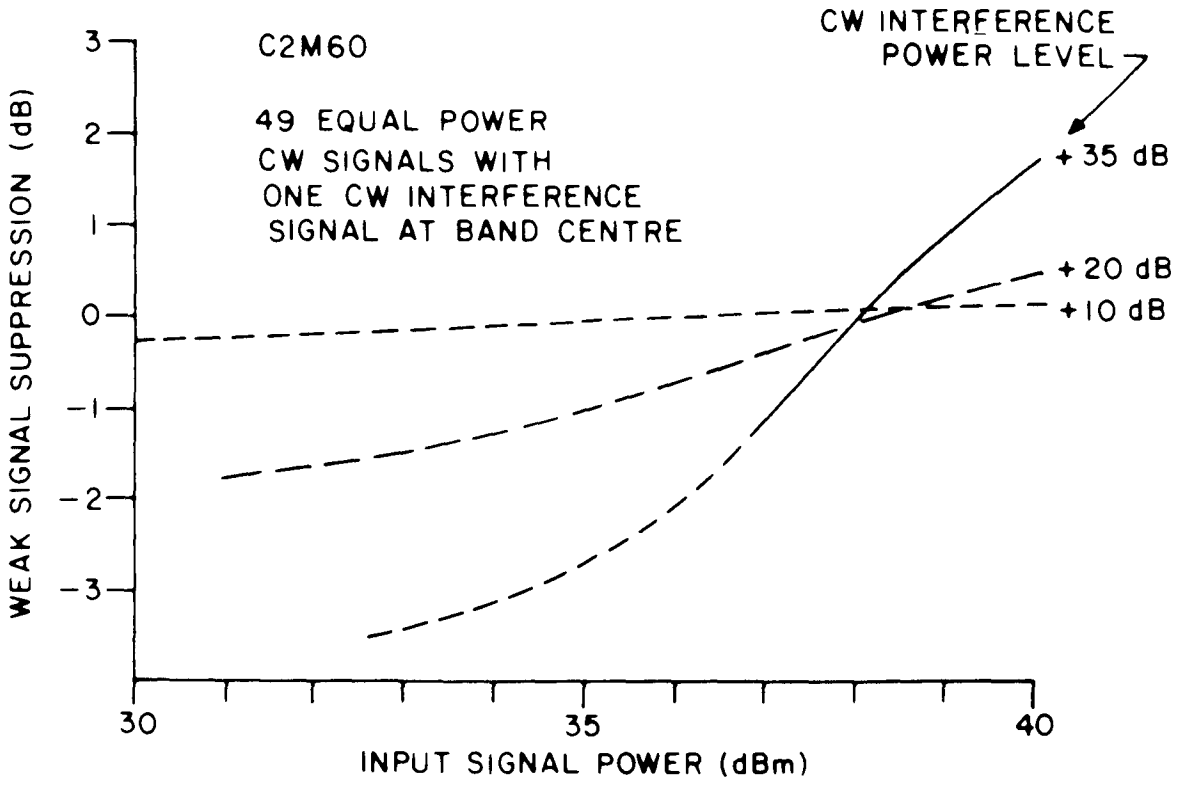


*Figure 29. C2M60 Weak Signal Suppression*

The remaining graphs in this section are output signal and intermodulation noise power spectra for the C2M60 amplifier operating at an input signal drive level of 39 dBm. The situation considered for Figure 30 is a block of twenty modulated signals. The power spectra for the channel with the worst S/IM performance is illustrated in this figure for the following three binary modulation cases:

1. frequency-shift-keying (FSK) with a deviation ratio of 0.7 (H = 0.7),
2. FSK, H = 0.5 (this is often referred to as fast FSK (FFSK),
3. anti-polar phase shift keying (PSK).

The power spectra of the various signals are generated and then the composite spectrum transformed into an autocorrelation function by use of a Fast Fourier transform subroutine.

Notice that the detailed intermodulation noise spectral shape is dependent upon the specific modulation technique used. Only the FSK, H = 0.7 gives rise to intermodulation noise which is relatively constant across the band. Reference back to Figure 28 shows the intermodulation noise level is slightly lower when modulated signals are considered.

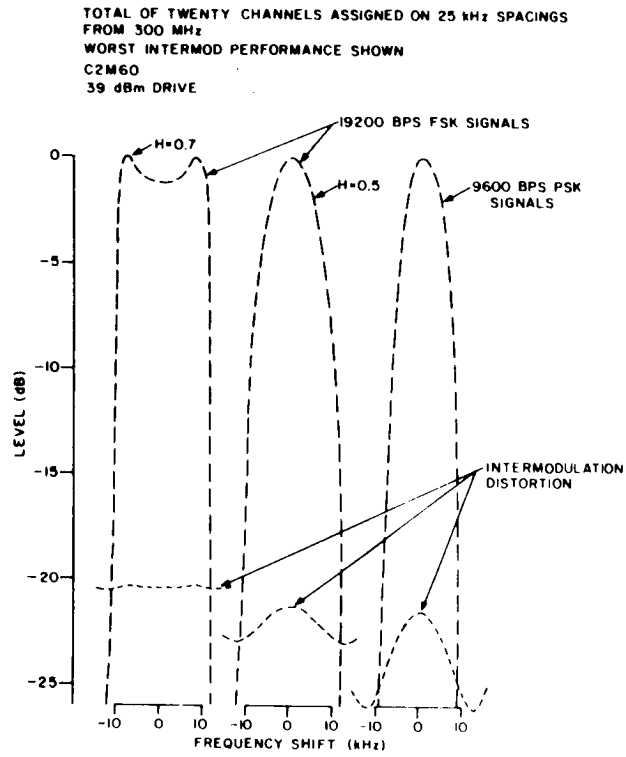


*Figure 30. Modulated Carriers*

For Figure 31 it was assumed the signal was a block of uniformly spaced carriers. Thus, intermodulation noise consists of carriers at all frequency shifts which are multiples of the spacing frequency. The spectrum illustrated is the envelope of the powers of the various sinusoidal components. This type of an analysis is identical to that used previously to generate the multiple-carrier S/IM performance curves.

The next sequence of three graphs, Figures 32 to 34, illustrates the S/IM performance behaviour when the individual carriers must be separated into two separate bands. The total overall bandwidth occupied by the two signal bands is identical to that used in Figure 31. Notice that as the two separate bands have a decreasing individual bandwidth the "ripple" on the intermodulation noise increases until the two bands are sufficiently narrow that a two sinusoid analysis would accurately model the situation. Certainly at this point the gaussian assumption of Section 3 should be queried.

To illustrate the capability of the computer programs to analyze signals which are not symmetrical about a centre reference frequency, the example of Figure 35 is presented. In this example there are three nonuniformly spaced bands of carriers. As would be expected, the intermodulation noise is nonsymmetric. Notice as well that there is "ripple" on the intermodulation noise as a result of the separate bands of carriers.

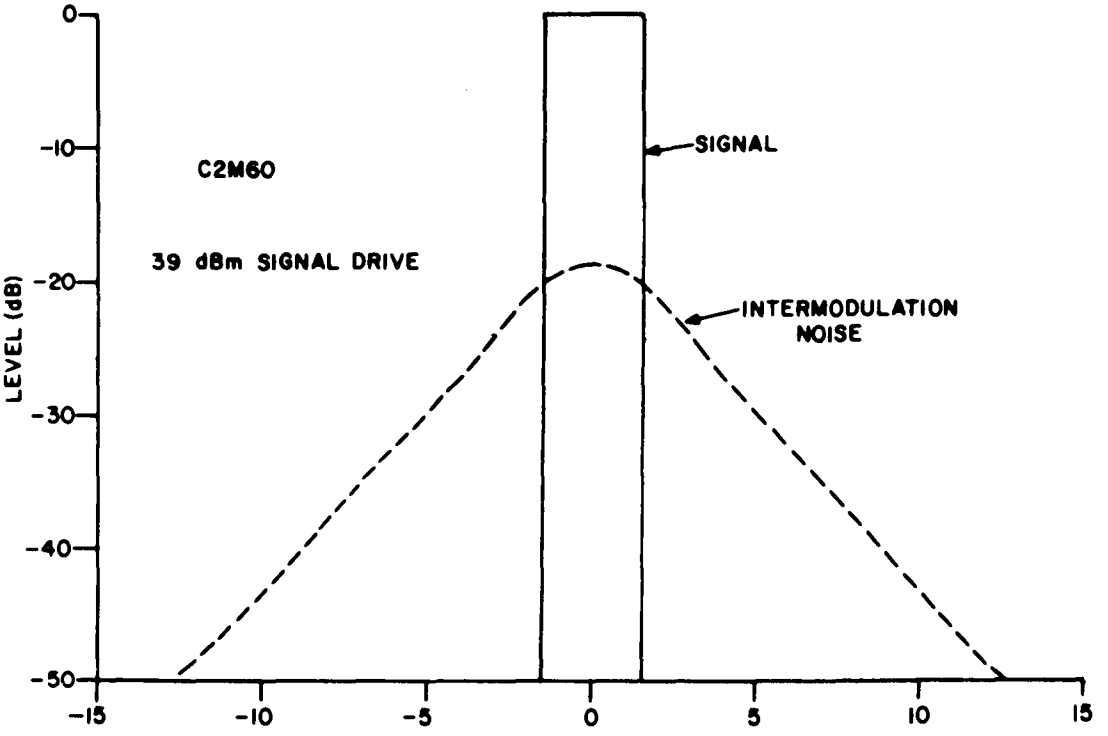


*Figure 31. Intermodulation Spectrum*

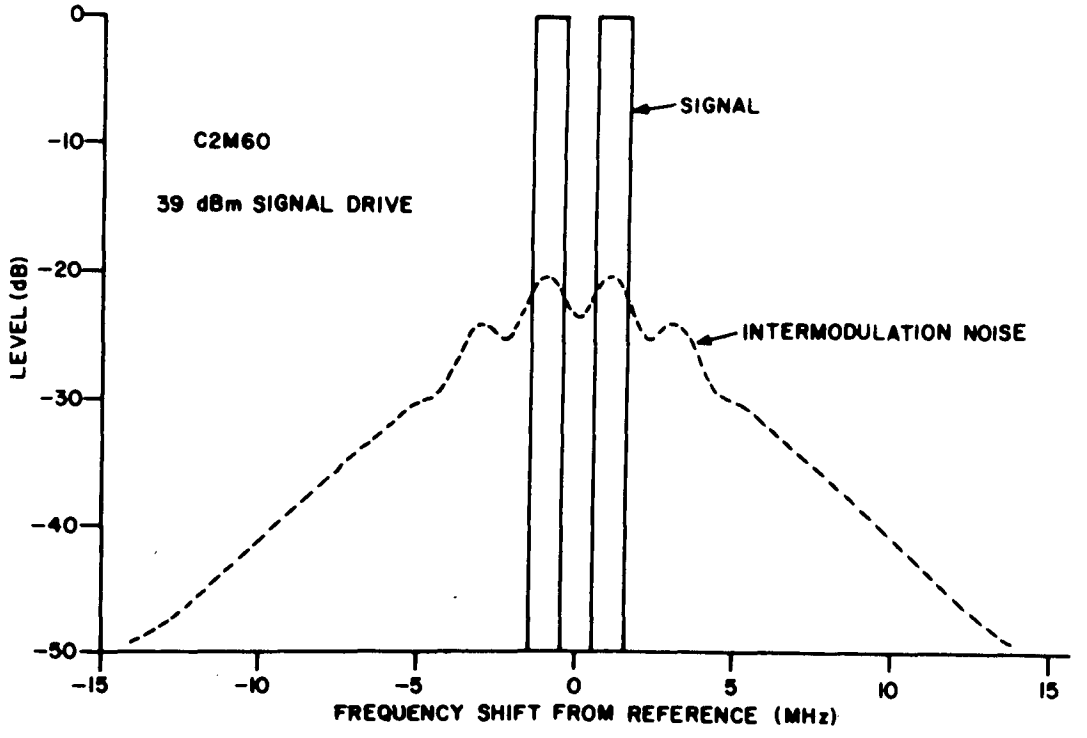


*Figure 32. 1st Twin Band Intermodulation Spectrum*

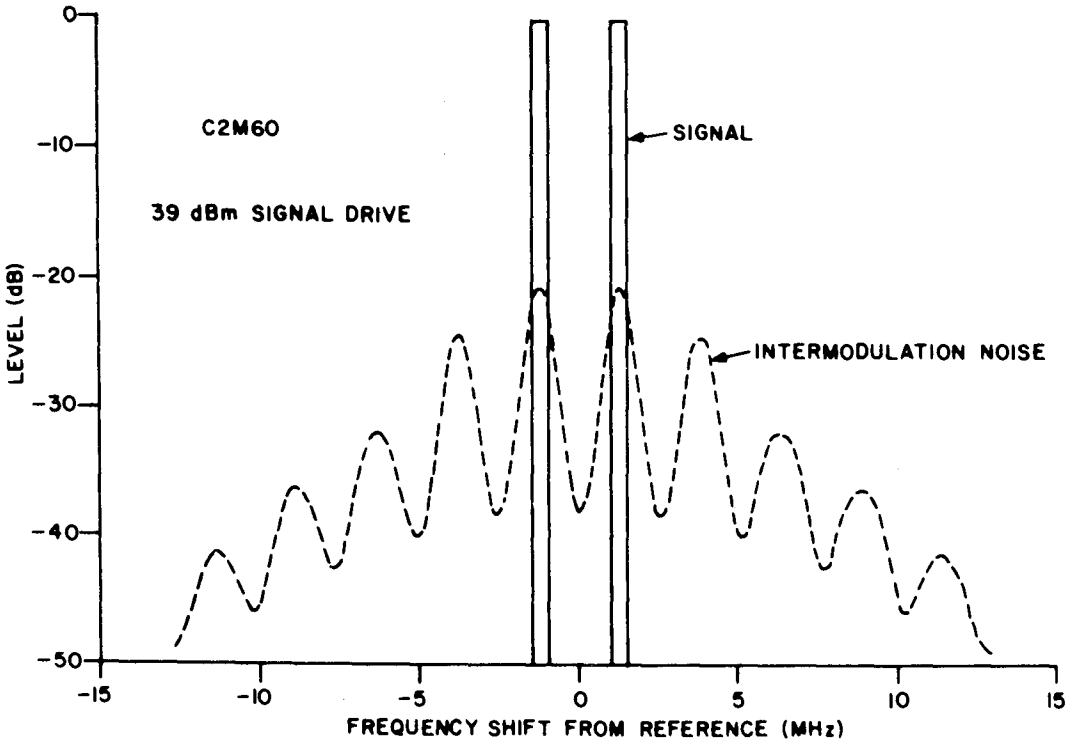


*Figure 33. 2nd Twin Band Intermodulation Spectrum*

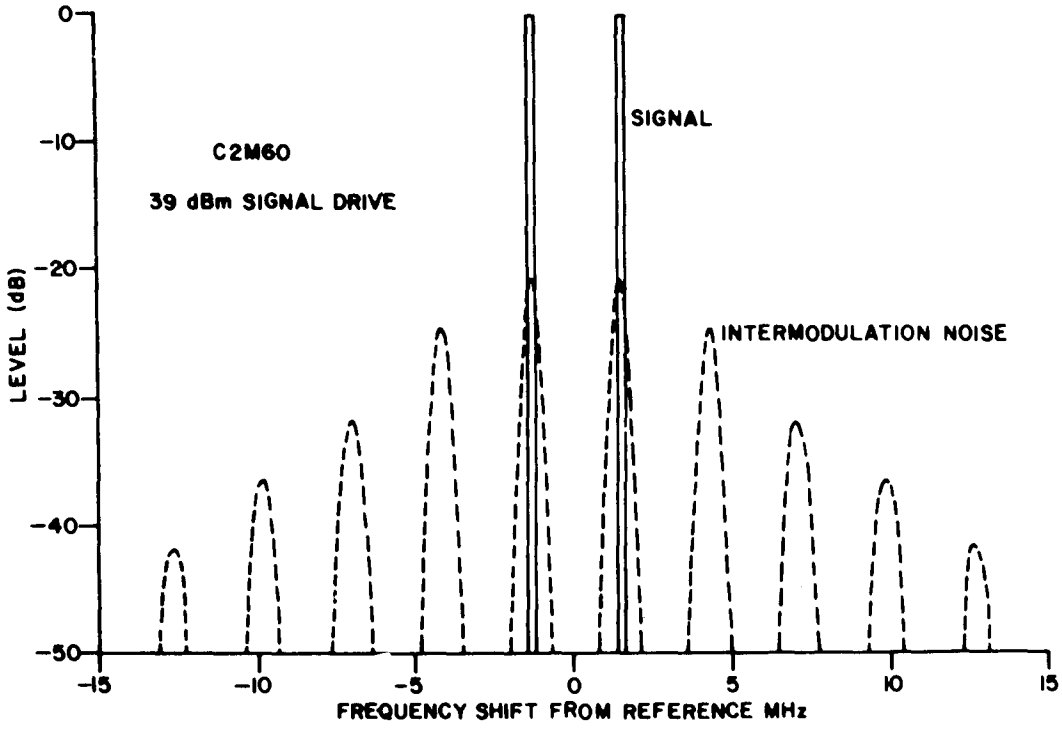


*Figure 34. 3rd Twin Band Intermodulation Spectrum*

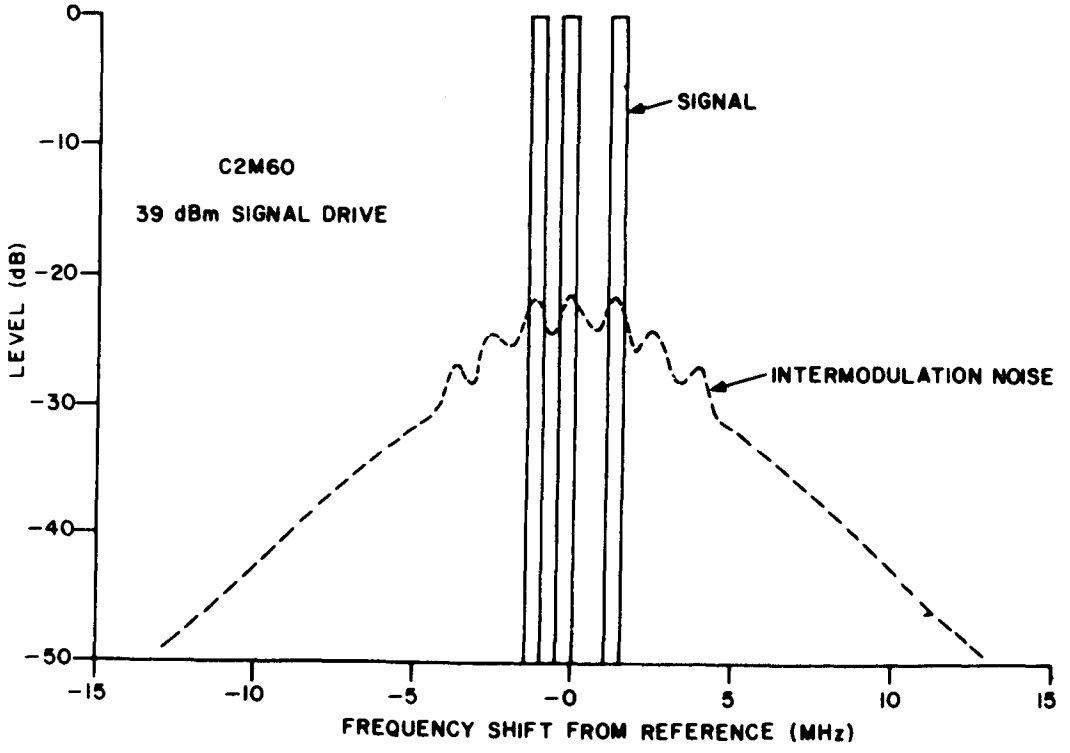


*Figure 35. Triple Band Intermodulation Spectrum*

A second example of nonsymmetrical spectrum type of signal is presented in Figure 36. In this case there are 85 carriers which constitute the main traffic through the transponder and a few high and low-powered signals. The nonsymmetrical intermodulation noise spectrum of Figure 36 results. A plot of the worst channel S/IM ratio versus the number of high-powered users is presented in Figure 37. The high-power channels have an excellent S/IM ratio; the normal and low-powered channels have approximately the same performance if there are 10 or fewer high-powered carriers.

The possible signal frequency assignments are countless and hence each particular case must be considered separately.

## 5.5 UHF SOLID STATE AMPLIFIERS - CLASS L

Various attempts have been made to improve the S/IM performance of nonlinear amplifiers. One approach currently being investigated by Welti [22] for use in the proposed INTELSAT V satellite TWTs is a feed forward compensation technique suggested by Seidal [23]. It is possible that such a technique might also be used with the UHF solid-state amplifiers discussed in this report.

A much simpler approach has been examined by Harrison and Moody [20] at RCA. They suggest that by introducing a slight amount of bias, as well as retuning the amplifier input and output filters, it is possible to significantly reduce the intermodulation noise level. For convenience, they have

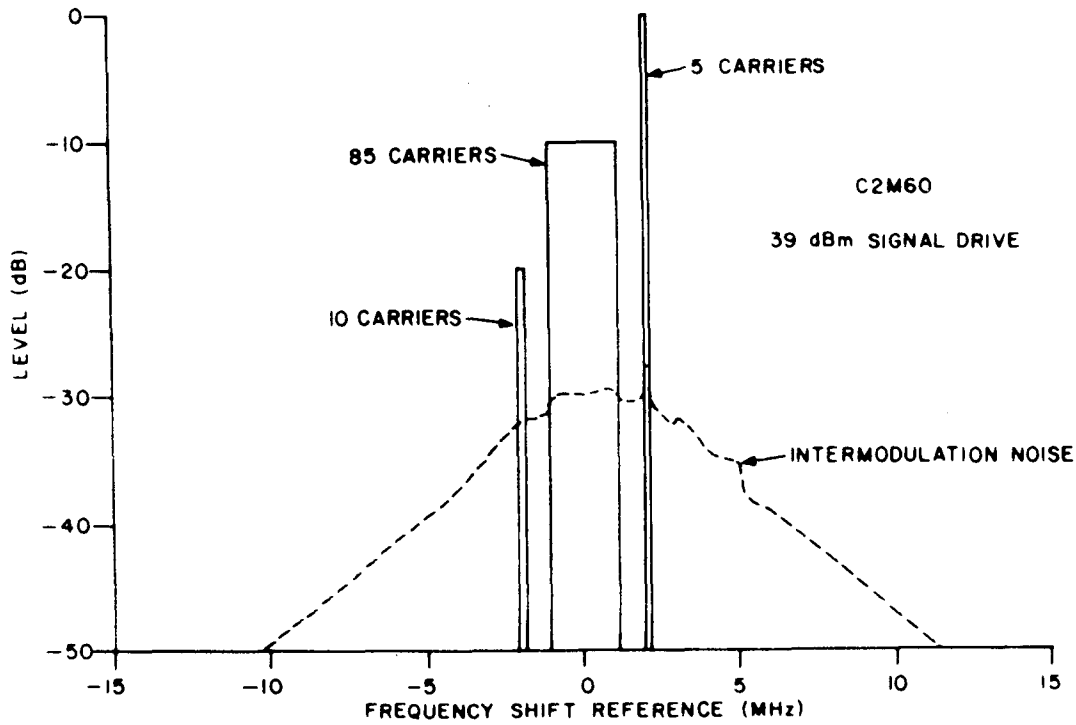


*Figure 36. Nonsymmetrical Signal Spectrum*

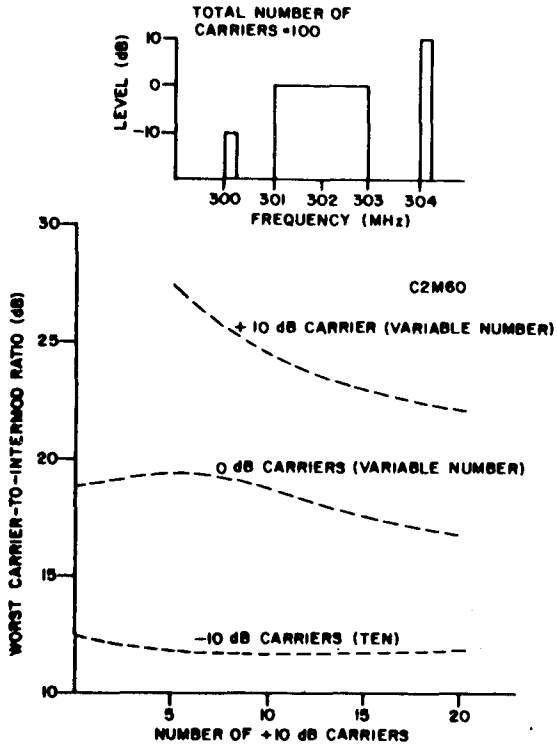


*Figure 37. Signal-to-Intermod Ratios*

called this mode of operation class "L" ("L" for low intermod). Preliminary work at CRC indicates that:

1. There is a definite bias value which *minimizes* the intermodulation noise without significantly changing the class C power efficiency of the amplifier.

2. There is only a trivial amount of power consumed by the amplifier when no signal is present.

3. The most significant adjustment parameter appears to be bias. The input and output filters do not necessarily have to be retuned.

The amount of improvement which can be expected is illustrated in Figures 38 to 40 for Harrison's CM75-28R transistor amplifier. The class C and class L performance of this amplifier is illustrated in Figure 38 and 39 respectively. From these two figures the performance improvement curves of Figure 40 have been generated. The penalty in prime-power efficiency refers to the change in efficiency percentage points.

No significant improvement can be expected, using this technique if excessive input signal drive levels are used (in excess of 40 dBm). From Figure 39 it is evident that the input signal drive should be of the order of 37 to 38 dBm if intermodulation noise is to be minimized. In this operating region an S/IM performance improvement of 9 to 11 dB can be expected with

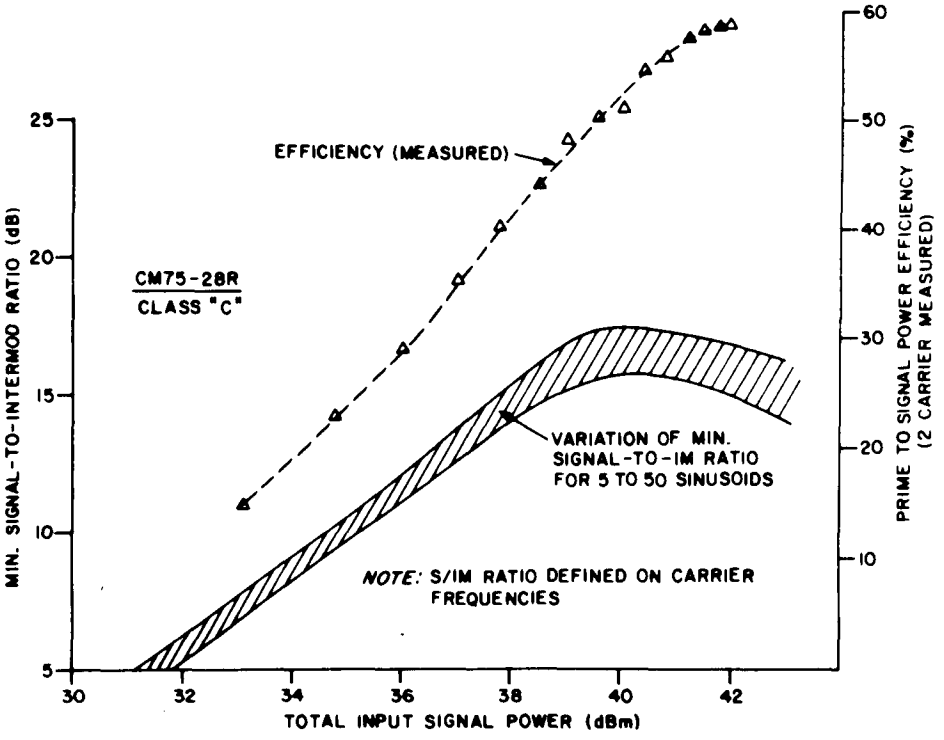


*Figure 38. CM75-28R Class-C Performance*

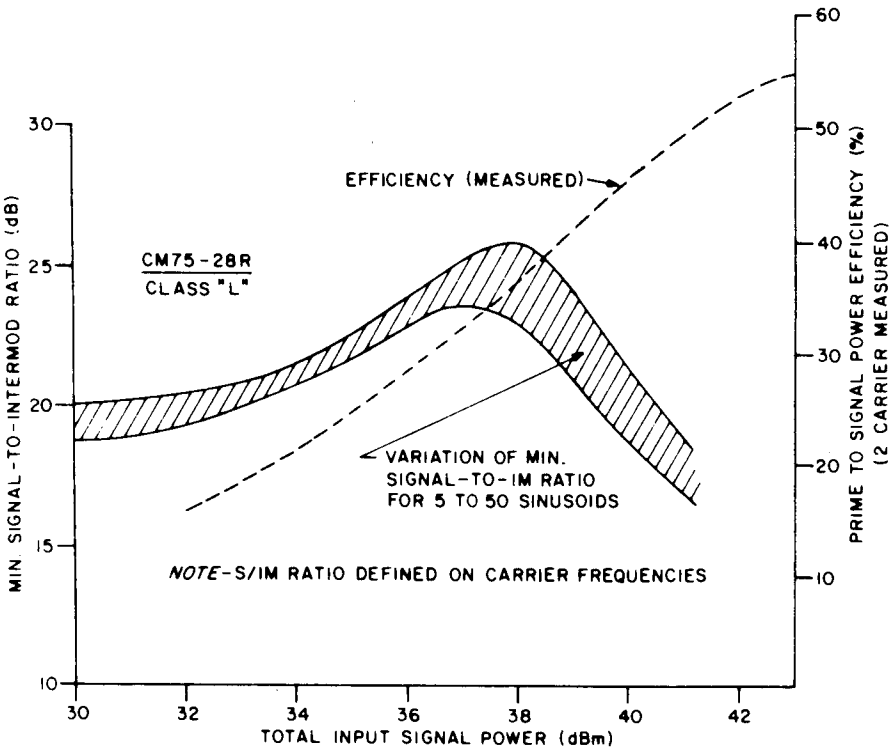


*Figure 39. CM75-28R Class–L Performance*

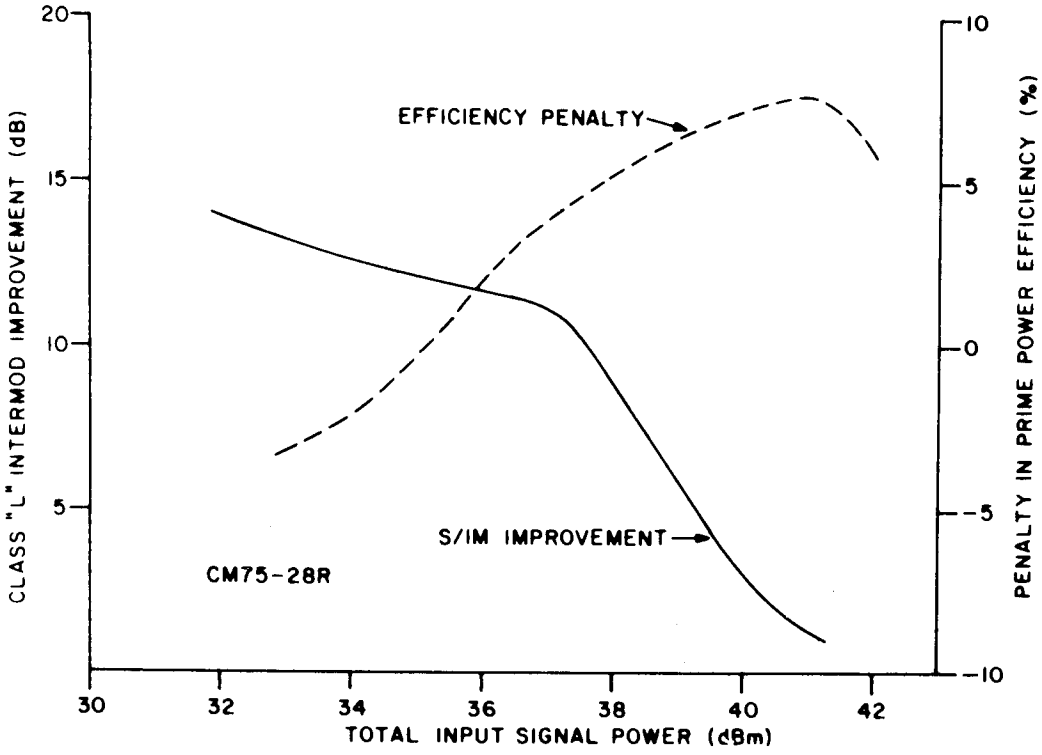


*Figure 40. Class-L Improvement*

only a 4 to 5 percentage point decrease in prime power efficiency. The amplifier's output signal power would then be of the order of 44 to 45 dB.

Although this technique of intermodulation noise reduction shows promise, it remains to develop an amplifier which can be used in an actual satellite transponder.

## 6. CONCLUDING REMARKS

The analysis presented in this report permits the prediction of signal and intermodulation noise at the output of actual TWT and solid-state class C UHF amplifiers. The analysis is intended for use in the study of the performance of FDMA satellite communication systems. The signals may be either sinusoidal carriers or modulated carriers of arbitrary power spectral shape.

For the situation where the composite signal is approximately gaussian in nature (i.e., there is a large number of individual users) an analysis technique which greatly reduces computation time is described. The analysis techniques have been applied in the performance study of TWT and solid-state UHF amplifiers. In the case of the solid-state amplifiers it is shown that a dynamic characteristic measurement technique must be used if reliable predictions are to be achieved.

The performance of a simple intermodulation noise reduction technique for solid-state UHF amplifiers is described. Useful improvements in signal to intermodulation noise ratios of 10 dB can be achieved while the amplifier efficiency is maintained within five percentage points of the equivalent class C amplifier.

## 7. ACKNOWLEDGEMENTS

The author is deeply indebted to Mr. D.L. Selin for his excellent work and assistance during the experimental phase of this study. Without his efforts the experimental phase of this study would not have been as successful as it was.

This work was sponsored by the Department of Defence, Research and Development Branch under Project 28-01-31.

## 8. REFERENCES

1. Rice, S.O., *Mathematical Analysis of Random Noise*, B.S.T.J., Volume XXIV, pp. 46-156, January 1945.

2. Davenport, W.B., and W.L. Root, *An Introduction to the Theory of Random Signals and Noise*, McGraw-Hill Book Company, 1958. pp. 277 - 311.

3. Eric, M.J., *Intermodulation Analysis of Nonlinear Devices for Multiple-Carrier Inputs*, CRC Technical Note Number 1234, Ottawa, Canada, November 1972.

4. Berman, A.L., and E.I. Podraczky, *Experimental Determination of Intermodulation Distortion Produced in a Wideband Communications Repeater*, IEEE International Conv. Rec., Volume 15, Pt. 2, pp. 69 - 88, 1967.

5. Baum, R.F., *The Correlation Function of Smoothly Limited Gaussian Noise*, IRE Trans. on Info. Theory, Volume IT-3, pp. 1I-3, pp. 193 - 197, September 1957.

6. Pawula, R.F., T.S. Fong, and M.R. O'Sullivan, *Intermodulation Distortion in Frequency Multiplexed Satellite Repeaters*, IEEE Proc., Volume 59, Number 2, pp. 213 - 218, February 1971.

7. Pawula, R.F., *The Effects of Quadratic AM-PM Conversion in Frequency-Division Multiple-Access Communication Satellite Systems*, IEEE Trans. on Com. Tech., Volume COM-19, Number 3, pp. 345 - 349, June 1971.

8. Davenport, Jr., W.B., *Signal-to-Noise Ratios in Bandpass Limiters*, Journal of Applied Physics, Volume 24, Number 6, pp. 720 - 727, June 1953.

9. Jones, J.J., *Hard-Limiting of Two Signals in Random Noise*, IEEE Trans. on Info. Theory, Volume IT-9, pp. 34 - 42, January 1963.

10. Shaft, P.D., *Limiting of Several Signals and Its Effect on Communication Performance*, IEEE Trans. on Com. Tech., Volume COM-13, Number 4, pp. 504 - 512, December 1965.

11. Shimbo, O., *Effects of Intermodulation, AM-PM Conversion, and Additive Noise in Multicarrier TWT Systems*, IEEE Proc., Volume 59, Number 2, pp. 230 - 238, February 1971.

12. Kaye, A.R., D.A. George and M.J. Eric, *Analysis and Compensation of Bandpass Nonlinearities for Communications*, IEEE Trans, on Com., Volume COM-20, Number 5, pp. 966 - 972, October 1972.

13. Fuenzalida, J.C., O. Shimbo and W.L. Cook, *Time-Domain Analysis of Intermodulation Effects Caused by Nonlinear Amplifiers*, COMSAT Tech. Rev., Volume 3, Number 1, pp. 89 - 143, Spring 1973.

14. Loo, C., *Calculation of Intermodulation Noise Due to Hard and Soft Limiting of Multiple Carriers*, ICC '74, Minneapolis, Minnesota, pp. 3A-1 - 3A-4.

15. Watson, G.N., *A Treatise on the Theory of Bessel Functions*, Cambridge University, 2nd Edition, 1966, p. 576.

16. Wittke, P.H., *On Frequency-Modulation Spectra and the Distribution of a Functional of the Modulating Process*, Queen's University Research Report Number 66-1, Kingston, Ontario.

17. Schwartz, M., W.R. Bennett and S. Stein, *Communication Systems and Techniques*, McGraw-Hill Book Co., 1966, p. 36.

18. Franks, L.E., *Signal Theory*, Prentice-Hall Inc., 1969, p. 196.

19. Wilde, D.J., and C.S. Beightler, *Foundations of Optimalization*, Prentice-Hall Incorporated, 1967, pp. 397 - 313.

20. Harrison, R.G., and H.J. Moody, *A Study of Low Intermodulation Transistor Power Amplifiers*, Final Report under contract number PZ.36001-3929 submitted to the Director General, Communications Research Centre, Department of Communications, Ottawa, May 1974.

21. Campbell, L.L., *Approximation of an Integral Connected with Hard-Limited Signals and Noise*, Queen's University Research Report Number 69-3, Department of Electrical Engineering, Queen's University, Kingston, Ontario, 1969, p. 3.

22. Welti, G.R., *Nonlinear Channels for Multicarrier Transmission*, presented at the NATO Advanced Study Institute on New Directions in Signal Processing in Communications and Control, 5 - 17 August 1974, Darlington, U.K.

23. Seidal, H., *A Microwave Feed-Forward Experiment*, B.S.T.J., 50, p. 2879, 1971.

24. Abramowitz M., and I.A. Stegun, *Handbook of Mathematical Functions*, Dover Publications Inc., June 1964.

# APPENDIX A

## Bessel Function Relationships

This appendix contains a summary of the basic Bessel function relationships used in the main development.

From Watson [18], p. 20, equation (5) Bessel's integral may be written as

$$J_n(z) = \frac{1}{2\pi} \int_{\alpha}^{2\pi+\alpha} \exp j(n\theta - z \sin\theta)\, d\theta \tag{A.1}$$

Let $n = 1$ and $\theta_2 = \theta - \pi/2$ in this equation to get

$$J_1(z) = \frac{1}{2\pi} \int_{\alpha_1}^{2\pi+\alpha_1} j \exp j(\theta_2 - z \cos\theta_2)\, d\theta_2 \tag{A.2}$$

Define $\eta-\beta = \theta_2$ and substitute this into equation (A.2). Thus

$$J_1(z) = \frac{1}{2\pi} \int_{\alpha_1+\beta}^{2\pi+\alpha_1+\beta} j \exp j\{\eta-\beta - z \cos(\eta-\beta)\}\, d\eta \tag{A.3}$$

Since $\beta$ is an arbitrary constant the limits of integration can be set by allowing $\alpha_1+\beta = -\pi$, to obtain the resulting relationship

$$J_1(z) = \frac{1}{2\pi} j \exp(-j\beta) \int_{-\pi}^{\pi} \exp j[\eta - z \cos(\eta-\beta)]\, d\eta \tag{A.4}$$

By a similar development it can be shown that

$$J_1(z) = \frac{1}{2\pi} j \exp(j\beta) \int_{-\pi}^{\pi} \exp j[-\eta - z \cos(\eta-\beta)]\, d\eta \tag{A.5}$$

A particular case of Weber's second exponential integral is given by Watson [18], p. 395, equation (1) as

$$\int_0^\infty \exp(-p^2t^2)J_\nu(at)J_\nu(bt)t\,dt = \frac{1}{2p^2}\exp\left(-\frac{a^2+b^2}{4p^2}\right)I_\nu\left(\frac{ab}{2p^2}\right) \tag{A.6}$$

provided $R(\nu) > -1$ and $|\arg p| < \pi/4$. This relationship is used in the text with $\nu = 1$ and $p = 1$.

Watson [18], p. 456, equation (1) presents an evaluation of Hankel's repeated integral as

$$\int_0^\infty udu \int_0^\infty F(R)J_\nu(uR)J_\nu(ur)RdR = \frac{1}{2}\{F(r+o) + F(r-o)\} \tag{A.7}$$

provided

$$\int_0^\infty F(R)\sqrt{R}\,dR \tag{A.8}$$

exists and is absolutely convergent; and the order of the Bessel functions is such that $\nu \geq -1/2$. The inversion of Hankel's repeated integral is given as

$$\int_0^\infty udu \int_0^\infty F(R)J_\nu(uR)J_\nu(ur)RdR = \lim_{\lambda\to\infty}\int_0^\infty F(R)\left\{\int_0^\lambda J_\nu(uR)J_\nu(ur)udu\right\}RdR \tag{A.9}$$

subject to the same constraints on $\nu$ and $F(R)$.

Another relationship which is used in the main development is Hankel's generalization of Weber's first exponential integral given by Watson [18], p. 393, equation (2) as

$$\int_0^\infty J_\nu(at)\exp(-p^2t^2)t^{\mu-1}\,dt = \frac{\Gamma\left(\frac{\nu+\mu}{2}\right)\left(\frac{a}{2p}\right)^\nu}{2p^\mu\,\Gamma(\nu+1)}\;{}_1F_1\left(\frac{\nu+\mu}{2};\,\nu+1;\,-\frac{a}{4p^2}\right) \tag{A.10}$$

where ${}_1F_1(\alpha;\rho;z)$ is a hypergeometric function which can be defined by

$${}_1F_1(\alpha;\rho;z) = \sum_{n=0}^{\infty}\frac{(\alpha)_n}{n!\,(\rho)_n}z^n \tag{A.11}$$

$$(\alpha)_n = \alpha(\alpha+1)(\alpha+2)\ \ldots\ (\alpha+n-1)$$

$$(\alpha)_o = 1$$

To secure convergence of the integral in (A.10) at the origin it is necessary that

$$R(\mu+\nu) > 0$$

A useful series expansion for the modified Bessel function is given by Watson [18], p. 77, equation (2) as

$$I_\nu(z) = \sum_{m=0}^{\infty} \frac{\left(\frac{1}{2} z\right)^{\nu+2m}}{m!\ \Gamma(\nu+m+1)} \tag{A.12}$$

The modified Bessel function is related to the Bessel function of the first kind by the following formula given by Abramowitz and Stegun [24], p. 375, equation (9.6.3)

$$I_\nu(z) = \exp - \frac{i\pi\nu}{2} J_\nu\left(ze^{\frac{\pi i}{2}}\right) \quad -\pi < \arg z \leq \frac{\pi}{2} \tag{A.13}$$

For $\nu = n$, an integer the formula reduces to

$$I_n(z) = \exp\left\{-\frac{n\pi}{2} i\right\} J_n(iz) \quad -\pi < \arg z \leq \frac{\pi}{2} \tag{A.14}$$

or

$$I_1(z) = iJ_1(iz) \tag{A.14b}$$

From p. 14 of Watson [15], Jacobi's expansion is given as

$$\exp\left\{\frac{1}{2} z \left(t - \frac{1}{t}\right)\right\} = \sum_{n=-\infty}^{\infty} t^n J_n(z) \tag{A.15}$$

If we define

$$t = \exp j\theta \tag{A.16}$$

then it follows directly that

$$\exp\{jz \sin\theta\} = \sum_{n=-\infty}^{\infty} J_n(z) \exp jn\theta \tag{A.17}$$

# APPENDIX B

## Gaussian Sinusoid Development

It has been shown in Section 3 (equation 3.12) that the autocorrelation function of $\overline{z}(t)$ can be expressed as

$$\overline{R}(\tau) = -\frac{1}{(2\pi)^2} \exp j\omega_o\tau \int_0^{\infty}\int_{-\pi}^{\pi}\int_0^{\infty}\int_{-\pi}^{\pi} \exp\left\{j(\beta_2-\beta_1)\alpha_1\alpha_2\, M_p(\alpha_1,\beta_1,\alpha_2,\beta_2)\, d\beta_1 d\beta_2 \right.$$

$$\left. \times \int_0^{\infty} \rho_1 J_1(\alpha_1\rho_1)\overline{g}^*(\rho_1)d\rho_1 \int_0^{\infty} \rho_2 J_1(\alpha_2\rho_2)\overline{g}(\rho_2)d\rho_2 d\alpha_1 d\alpha_2 \right. \tag{B.1}$$

where the range of integration for $\beta_1$, $\beta_2$ is from $-\pi$ to $\pi$ and 0 to $\infty$ for all other integration variables. The other quantities of interest in this expression are defined as follows:

$$\overline{g}^*(\rho) = \text{complex conjugate of } \overline{g}(\rho)$$

$$M_p(\alpha_1,\beta_1,\alpha_2,\beta_2) = \text{a polar coordinate version of } M(\lambda_1,\xi_1,\lambda_2,\xi_2)$$

$$M(\lambda_1,\xi_1,\lambda_2,\xi_2) = E[\exp\{j\lambda_1 x_1 + j\xi_1 y_1 + j\lambda_2 x_2 + j\xi_2 y_2\}] \tag{B.2}$$

$$= \text{the joint characteristic function of } x_1, y_1, x_2, y_2$$

where

$$x_1 = x(t) \qquad y_1 = y(t)$$

$$x_2 = x(t+\tau) \qquad y_2 = y(t+\tau) \tag{B.3}$$

$$E[a] = \text{expected value of "a"}$$

The rectilinear-to-polar-coordinate conversion is defined by

$$\lambda_1 = \alpha_1 \cos\beta_1 \qquad \xi_1 = \alpha_1 \sin\beta_1$$

and (B.4)

$$\lambda_2 = \alpha_2 \cos\beta_2 \qquad \xi_2 = \alpha_2 \sin\beta_2$$

The objective of this appendix is to simplify equation (B.1) when the composite input signal consists of a sum of independent sinusoids.

For the moment consider the evaluation of just the joint characteristic function in equation (B.1). It has been shown in Section 3 (equation 3.27) that when there is a large number of users accessing the satellite, the joint characteristic function can be expressed as

$$M_p(\alpha_1,\beta_1,\alpha_2,\beta_2) = \exp\left[-\frac{1}{2}\left\{\phi_x(o)[\alpha_1^2+\alpha_2^2] + 2\alpha_1\alpha_2[\phi_x(\tau)\cos(\beta_1-\beta_2) + \phi_y(\tau)\sin(\beta_1-\beta_2)]\right\}\right] \quad (B.5)$$

given that the autocorrelation function of the composite input signal is represented by

$$R(\tau) = \phi_x(\tau)\cos\omega_o\tau + \phi_y(\tau)\sin\omega_o\tau \quad (B.6)$$

Because of the assumed independence of the individual signals at the amplifier's input, equation (B.6) can also be written as

$$R(\tau) = \sum_{i=1}^{N} R_i(\tau) \quad (B.7)$$

where

$$R_i(\tau) = \phi_i(\tau)\cos(\omega_o+\omega_i)\tau \quad (B.8)$$

$R_i(\tau)$ is the autocorrelation function of the signal from the $i^{th}$ user. In the analysis presented here it is assumed the system noise can be ignored.

From equations (B.6) to (B.8) it is evident that

$$\phi_x(\tau) = \sum_{i=1}^{N} \phi_i(\tau)\cos\omega_i\tau \quad (B.9)$$

$$\phi_y(\tau) = -\sum_{i=1}^{N} \phi_i(\tau)\sin\omega_i\tau \quad (B.10)$$

Substitution of equations (B.9) and (B.10) into the general expression of equation (B.5) gives the joint characteristic function as

$$M_p(\alpha_1,\beta_1,\alpha_2,\beta_2) = \prod_{i=1}^{N} \exp\left[-\frac{1}{2}\left\{\phi_i(o)[\alpha_1^2+\alpha_2^2] + 2\alpha_1\alpha_2\phi_i(\tau)\cos[\omega_i\tau+\beta_1-\beta_2]\right\}\right] \quad (B.11)$$

At this point in the development it is possible to make use of an approximation given by Campbell [21] to write an approximation of equation (B.11) as

$$M_p(\alpha_1,\beta_1,\alpha_2,\beta_2) = \prod_{i=1}^{N} J_o\left\{(2\phi(o)[\alpha_1^2 + \alpha_2^2] + 4\alpha_1\alpha_2\phi_i(\tau)\cos[\omega_i\tau + \beta_1-\beta_2)]\right\}^{\frac{1}{2}} \tag{B.12}$$

This approximation has also been used by Shimbo [11] in his work.

At this point it is necessary to restrict the development to the situation where the composite input signal is a sum of sinusoids. In this situation

$$\phi_i(o) = \frac{A_i^2}{2} = \phi_i(\tau) \tag{B.13}$$

It is now possible to make use of a Bessel function expansion given by Watson [15] as

$$J_o\left\{\sqrt{\zeta^2 + z^2 - 2z\,\zeta\cos\phi}\right\} = \sum_{m=-\infty}^{\infty} J_m(\zeta)J_m(z)\exp mj\phi \tag{B.14}$$

This expansion can be applied to equation (B.2) if

$$\zeta = \alpha_1 A_i \qquad z = \alpha_2 A_i \qquad \phi = \omega_i\tau + \beta_1-\beta_2 \tag{B.15}$$

hence

$$M_p(\alpha_1,\beta_1,\alpha_2,\beta_2) = \prod_{i=1}^{N}\sum_{m=-\infty}^{\infty} (-1)^m J_m(\alpha_1 A_i)J_m(\alpha_2 A_i)\exp\{jm(\omega_i\tau + \beta_1\beta_2\} \tag{B.16}$$

This product of a summation can be expressed as a sum of each of the individual product terms as shown in the following shortened form:

$$M_p(\alpha_1,\beta_1,\alpha_2,\beta_2) = \sum_{m=-\infty}^{\infty}\prod_{i=1}^{N} (-1)^{m_i} J_{m_i}(\alpha_1 A_i)J_{m_i}(\alpha_2 A_i)\exp\{jm_i(\omega_i\tau + \beta_1-\beta 2)\} \tag{B.17}$$

It is implicit in this expression that each $m_i$ goes through the allowed range of values and the various product terms summed. The expression in equation (B.17) can be simplified further and the joint characteristic function expressed as

$$M_p(\alpha_1,\beta_1,\alpha_2,\beta_2) = \sum_{m_i=-\infty}^{\infty} (-1)^{\sum_{i=1}^{N} m_i} \exp\left\{j\sum_{i=1}^{N} m_i\omega_i\tau\right\} \exp\left\{j\sum_{i=1}^{N} m_i(\beta_1-\beta_2)\right\}$$

$$\times \prod_{i=1}^{N} J_{m_i}(\alpha_1 A_i)J_{m_i}(\alpha_2 A_i) \tag{B.18}$$

This expression for the characteristic function can now be substituted into equation (B.1) and the integration with respect to $\beta_1$ and $\beta_2$ performed. If just the terms containing either $\beta_1$ or $\beta_2$ are considered the two integrals of interest can be written as

$$\int_{\pi}^{\pi} \exp\left\{j\left(\sum_{i=1}^{N} m_i - 1\right)\beta_1\right\} d\beta_2 \int_{\pi}^{\pi} \exp\left\{j\left(1 - \sum_{i=1}^{N} m_i\right)\beta_2\right\} d\beta_1 \qquad (B.19)$$

It is evident that both of these integrals are zero except when

$$\sum_{i=1}^{N} m_i = 1 \qquad (B.20)$$

in which case expression (B.19) has the value $(2\pi)^2$. This constraint should not be confused with the order of a particular intermodulation component which is defined by:

$$IMO = \sum_{i=1}^{N} |m_i| \qquad (B.21)$$

Incorporation of equation (B.18), the constraints of equation (B.20) and the evaluation of the integrals (B.19) into equation (B.1) simplifies the autocorrelation function of $\bar{z}(t)$ to

$$\bar{R}(\tau) = \sum_{m_i=-\infty}^{\infty} \exp j\left\{\omega_o \tau + \sum_{i=1}^{N} m_i \omega_i \tau\right\} \left| \int_0^{\infty} \alpha \prod_{i=1}^{N} J_{m_i}(\alpha A_i) \times \int_0^{\infty} \rho J_1(\alpha\rho)\bar{g}(\rho) d\rho d\alpha \right|^2 \qquad (B.22)$$

At this point in the development it is useful to model the nonlinear amplifier by a Bessel-Fourier series expansion defined by

$$\bar{g}(\rho) = \sum_{k=1}^{\infty} a_k J_1\{\Omega_k \rho\} \qquad (B.23)$$

where

$a_k$ are complex coefficients

$\{\Omega_k : k = 1,2,\ldots\}$ denoting either the set of positive zeros of $J_1(x)$ or $(2k - 1)\pi$ depending upon which series expansion is desired.

If this series expansion is substituted for $\bar{g}(\rho)$ in equation (B.22), the resulting Hankel's repeated integral can be evaluated as discussed in Appendix A. The resulting autocorrelation function is

$$\bar{R}(\tau) = \sum_{m_i=-\infty}^{\infty} \exp j\left\{\omega_o \tau + \sum_{i=1}^{N} m_i \omega_i \tau\right\} \left| \sum_{k=1}^{\infty} a_k \prod_{i=1}^{N} J_{m_i}\left\{\Omega_k A_i\right\} \right|^2 \tag{B.24}$$

If it is recalled at this point that the composite output signal from the amplifier is defined as

$$y(t) = \mathrm{Re}[\bar{z}(t)]$$

the autocorrelation function of the output signal is

$$R(\tau) = \sum_{m_i=-\infty}^{\infty} \frac{1}{2} \left| \sum_{k=1}^{\infty} a_k \prod_{i=1}^{N} J_{m_i}\left\{\Omega_k A_i\right\} \right|^2 \cos\left\{\omega_o \tau + \sum_{i=1}^{N} m_i \omega_i \tau\right\} \tag{B.25}$$

From equation (B.25) it is evident that the magnitude of a frequency component defined by the set $\{m_i: 1,2,\ldots N\}$ is given by the magnitude of

$$M(m_i: i = 1,2,\ldots,N) = \sum_{k=1}^{\infty} a_k \prod_{i=1}^{N} J_{m_i}\left\{\Omega_k A_i\right\} \tag{B.26}$$

These various frequency components add together on a power basis.

In the evaluation of a magnitude given in equation (B.26) it is necessary to evaluate a Bessel function value for each $m_i$ term. This evaluation can be very time consuming on a digital computer. Fortunately, the computation can be simplified if the approximation given by Campbell [21] is applied to those terms for which $m_i = 0$. Define

$$\{m_o\} = \{m_i: m_i = 0;\ i = 1,2,\ldots,N\} \tag{B.27}$$

and

$$\{m\} = \{m_i: m_i \neq 0;\ i = 1,2,\ldots,N\}$$

Equation (29) can now be simplified to

$$M(m_i: i = 1,2,\ldots,N) = \sum_{k=1}^{\infty} a_k \exp\left\{\frac{-\Omega_k^2}{4} \sum_{\{m_o\}} A_i^2\right\} \times \prod_{\{m\}} J_{m_i}\left\{\Omega_k A_i\right\} \tag{B.28}$$

Equations (B.25) to (B.28) form the basis for a sinusoidal intermodulation analysis. These equations are the same as the equations developed in Section 2.

# A P P E N D I X C

## Equipment List

| | |
|---|---|
| $G_1$ | HP 8640B signal generator |
| $G_2$ | Singer SG-1000 generator with external modulation capability |
| $G_3, G_4, G_5, G_6$ | Damon voltage-controlled crystal oscillators, type 6805 WXA |
| $A_1$ | WG RT-1 variable attenuator |
| AMP | MPD model LWA 055-4, 4-watt linear amplifier followed by a 1 KW linear RF power amplifier MCL model D10092 |
| F | Teleonic TBP 3-section bandpass filter, centre frequency 300 MHz bandwidth 30 MHz |
| $K_1, K_2$ | Narda Microline 3020A - 20 dB coupler |
| C | Microwave Associates G-3323-S circulator, 100 W |
| M | Pacific Measurements Incorporated peak reading power meter, type 1018 |
| PS | HP222A pulse stretcher |
| HC | HP8411A harmonic frequency converter |
| NA | HP8410A network analyzer with a type 8412A phase-magnitude display unit |
| $I_1 I_2$ | Anzac "Iso-T" TU-50, 200 - 400 MHz |
| PG | HP8005 pulse generator |
| MX | HP10514A mixer |
| SC | Olektron Power Combiner B-HJ-404X |
| SA | HP8555A Spectrum analyzer |

# CRC DOCUMENT CONTROL DATA

1. ORIGINATOR: Department of Communications/Communications Research Centre

2. DOCUMENT NO: CRC Report No. 1284

3. DOCUMENT DATE: February 1976

4. DOCUMENT TITLE: Intermodulation Analysis with Fourier-Bessel Expansions

5. AUTHOR(s): J.L. Pearce

6. KEYWORDS: (1) Intermodulation
(2) Fourier-Bessel Expansions
(3)

7. SUBJECT CATEGORY (FIELD & GROUP: COSATI)

17 Navigation, Communications, Detection, and Countermeasures

17 02 Communications

8. ABSTRACT:

In any frequency-division-multiple-access (FDMA) satellite communications system the control of intermodulation noise must be considered if all signals are amplified by a single nonlinear power amplifier in the satellite transponder.

The subject of this report is the use of Fourier-Bessel series expansion models in the prediction of the intermodulation performance of both travelling-wave-tube (TWT) amplifiers and solid state class C, UHF amplifiers. Both theoretical and experimental results are described and compared.

It is shown that in the case of the solid state amplifiers a dynamic characteristic measurement technique must be used before reliable predictions can be achieved. A simple intermodulation noise reduction scheme is described for use with high-power-efficiency-class-C solid state amplifiers. It is demonstrated that a signal-to-intermodulation noise power ratio improvement of 10 dB can be achieved with a minimal decrease in prime power efficiency.

9. CITATION:

PEARCE, JOHN L.
--Intermodulation analysis with
Fourier-Bessel expansions.

TK
5102.5
.C673e
#1284

DATE DUE
DATE DE RETOUR

| | | | |
|---|---|---|---|
| | | | |
| | | | |
| | | | |
| | | | |
| | | | |
| | | | |
| | | | |
| | | | |
| | | | |
| | | | |
| | | | |
| | | | |
| | | | |
| | | | |
| | | | |
| | | | |
| | | | |
| | | | |
| | | | |

LOWE-MARTIN No. 1137

INDUSTRY CANADA / INDUSTRIE CANADA
209160